

AD-777 881

MICROWAVE HERTZIAN GENERATOR
INVESTIGATION

W. H. McNeill, et al

IKOR, Incorporated

Prepared for:

Rome Air Development Center

March 1974

DISTRIBUTED BY:

NTIS

National Technical Information Service
U. S. DEPARTMENT OF COMMERCE
5285 Port Royal Road, Springfield Va. 22151

UNCLASSIFIED

SECURITY CLASSIFICATION OF THIS PAGE (When Data Entered)

REPORT DOCUMENTATION PAGE		READ INSTRUCTIONS BEFORE COMPLETING FORM	
1. REPORT NUMBER RADC-TR-74-33	2. GOVT ACCESSION NO.	3. RECIPIENT'S CATALOG NUMBER <i>AD 777881</i>	
4. TITLE (and Subtitle) MICROWAVE HERTZIAN GENERATOR INVESTIGATION		5. TYPE OF REPORT & PERIOD COVERED Final Technical Report 15 May 1972 - 30 Nov 1973	
		6. PERFORMING ORG. REPORT NUMBER	
7. AUTHOR(s) W. H. McNeill J. M. Proud		8. CONTRACT OR GRANT NUMBER(s) F30602-72-C-0387	
9. PERFORMING ORGANIZATION NAME AND ADDRESS IKOR Inc. Northeast Industrial Park Burlington, MA 01803		10. PROGRAM ELEMENT, PROJECT, TASK AREA & WORK UNIT NUMBERS 55730374	
11. CONTROLLING OFFICE NAME AND ADDRESS Rome Air Development Center (OCTP) Griffiss Air Force Base, New York 13441		12. REPORT DATE March 1974	
		13. NUMBER OF PAGES 73	
14. MONITORING AGENCY NAME & ADDRESS (if different from Controlling Office) Same		15. SECURITY CLASS. (of this report) Unclassified	
		15a. DECLASSIFICATION DOWNGRADING SCHEDULE N/A	
16. DISTRIBUTION STATEMENT (of this Report) Approved for public release; distribution unlimited.			
17. DISTRIBUTION STATEMENT (of the abstract entered in Block 20, if different from Report) Same			
18. SUPPLEMENTARY NOTES RADC Project Engineer: William C. Quinn			
19. KEY WORDS (Continue on reverse side if necessary and identify by block number) Electronics and Electrical Engineering Subsystem Conversion Techniques Wave Propagation Reproduced by NATIONAL TECHNICAL INFORMATION SERVICE U S Department of Commerce Springfield VA 22151			
20. ABSTRACT (Continue on reverse side if necessary and identify by block number) A program has been conducted to investigate the feasibility of a microwave version of the frozen wave generator. An approach using ultraviolet triggered spark gap switches is reported which successfully demonstrates the operating principles of the generator at frequencies below 1 GHz. The investigation includes a study of UV triggering phenomena in overvolted spark gaps.			

DD FORM 1473
1 JAN 73

EDITION OF 1 NOV 65 IS OBSOLETE

UNCLASSIFIED

SECURITY CLASSIFICATION OF THIS PAGE (When Data Entered)

MICROWAVE HERTZIAN GENERATOR INVESTIGATION

W. H. McNeill
J. M. Proud

IKOR Incorporated

Approved for Public Release;
Distribution Unlimited.

Do not return this copy.
Retain or destroy.

1a

FOREWORD

This final report covering the period 15 May 1972 to 30 November 1973 was prepared by IKOR Incorporated, Northwest Industrial Park, Burlington, Massachusetts, under Contract F30602-72-C-0307, Project No. 55730374. Mr. William Quinn(OCTP) was the RADC project engineer.

This report has been reviewed by the Office of Information, RADC, and approved for release to the National Technical Information Service (NTIS).

This report has been reviewed and is approved.

APPROVED:



WILLIAM C. QUINN
Project Engineer



APPROVED:

WILLIAM T. POPE
Assistant Chief
Surveillance and Control Division

FOR THE COMMANDER:



CARLO P. CROCETTI
Chief, Plans Office

EVALUATION

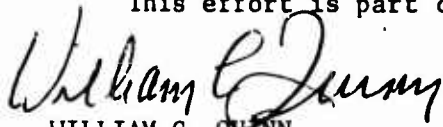
Project: 5573
Contract No: F30602-72-C-0387
Effort Title: Microwave Hertzian Generator Investigation

Contractor: IKOR Inc
Northeast Industrial Park
Burlington, MA 01803

Hertzian transmitters in general show promise for simple, reliable, low cost, high power, microwave generation devices at very short pulse durations eg. ten r.f. cycles. In addition, the frozen wave principle offers the opportunity for very high conversion efficiency, perhaps 60% or better.

While the frozen wave concept is simple and straightforward in principle, successful operation at a given frequency requires simultaneous closing of several switches within a time span small compared to one r.f. period. It follows that exploitation of the frozen wave principle in the microwave region will depend upon how well this criteria can be met at increasingly higher frequencies. The present study was concerned almost exclusively with u.v. synchronized overvolted spark gaps as the switch element. While no precise upper frequency limit can be stated, this study has shown that acceptable operation can be expected up to approximately 500 MHz with this switching technique. At one gigahertz and above, the need for a substantially better synchronization technique is clearly indicated.

This effort is part of RADC Technology Plan TPO 5 .



WILLIAM C. QUINN
RADC/OCTP

TABLE OF CONTENTS

<u>Section</u>	<u>Title</u>	<u>Page</u>
I	INTRODUCTION	1
II	FROZEN WAVE GENERATOR DESIGN CONCEPTS	3
III	SPARK GAP PHENOMENA AND POWER LIMITS	27
IV	EXPERIMENTAL GENERATORS	43
V	SUMMARY AND RECOMMENDATIONS	63

LIST OF ILLUSTRATIONS

<u>Figure</u>	<u>Title</u>	<u>Page</u>
1.	Weibel's Frozen Wave Generator	4
2.	Basic Frozen Wave Generator	7
3.	Basic Generator with Single Wave Output	8
4.	Sine Wave Approximation	9
5.	Analyzed Wave Shapes	11
6.	A Curved Stripline Generator	20
7.	Schematic of A Folded Line Generator	22
8.	Input Pulse Charging Circuits	25
9.	UV Triggering Experiment	29
10.	UV Triggering Statistics vs. Optical Path	30
11.	UV Triggering Statistics vs. Field Strength	32
12.	UV Triggering Statistics	33
13.	Breakdown Field Strength vs. Applied Field Rise Time	37
14.	Rise Time Dependent Breakdown Study	39
15.	Preliminary Generator Electrical Schematic	44
16.	Preliminary Curved Line Generator	45
17.	Ten Cycle, Folded Line Generator	47
18.	Coaxial Frozen Wave Generator	50

LIST OF ILLUSTRATIONS

<u>Figure</u>	<u>Title</u>	<u>Page</u>
19.	Single Cycle Generator	51
20.	Three Cycle Unipolar Generator	54
21.	Four Cycle Unipolar Generator	55
22.	Two Cycle Bipolar Generator	57
23.	Four Cycle Bipolar Generator	58
24.	Five Cycle Bipolar Generator	59
25.	Eight Cycle Bipolar Generator	61
26.	Eight Cycle 500 MHz Generator	62

SECTION I INTRODUCTION

The purpose of the investigation reported here was to develop a microwave Hertzian generator based upon the "frozen wave" principle. The generation scheme is extremely simple in concept and involves a two-step process whereby a static or "frozen" electric field profile is established in a sectioned transmission line and is subsequently released by rapidly switching all of the sections into series connection. In addition to the feature of simplicity, the frozen wave generator offers considerable promise for high efficiency. While the concept is not a new one, the prior development was conducted at low frequencies near one megahertz. This earlier work was performed with lumped parameter transmission lines and triggered spark gap switching techniques which have existed in the capacitor energy storage and discharge field for some time.

Recent advances in the understanding and application of nanosecond and subnanosecond spark gap switch phenomena, coupled with modern distributed parameter transmission line methods offer the promise that the frozen wave generator can be extended to the microwave frequency domain. The investigation reported here embraces both facets of the extension. Of paramount importance in the higher frequency domain is the need to attain the ability to close the multiple switches in the generator with a high degree of simultaneity and fast rates of closure. The approach has been to exploit the fast closure properties of highly overvolted spark gaps while achieving synchronization through optical triggering with ultraviolet light.

The investigation has encompassed a study to define various device design approaches including an analysis of the switching requirements. Following this, an experimental study of the UV triggered spark gap was undertaken to provide a design data base and to enable a quantitative theoretical evaluation of factors which ultimately limit performance.

Several breadboard model frozen wave generators have been investigated in this program, reinforcing the promise of achieving a higher frequency device. The program was particularly successful in achieving performance at 250 MHz,

constituting a two order of magnitude extension of the prior art in the frequency domain. While lesser success was reached at 500 MHz and 1.3 GHz, the difficulties at these and yet higher frequencies have been identified as have been the directions for improvement.

SECTION II

FROZEN WAVE GENERATOR DESIGN CONCEPTS

This section reviews design concepts of the frozen wave generator which have served as the foundation for the laboratory effort in this program. The following paragraphs discuss the basic concept as originally developed by Weibel⁽¹⁾ and Lietti⁽²⁾. Subsequently, the design transition to the higher frequency domain of interest in this program is reviewed, including an analysis of high power switch requirements. Finally, implementation approaches are considered.

1. PRIOR ART - LUMPED ELEMENT GENERATORS

The frozen wave generator was initially developed^(1, 2) as a high power rf source operating near 1 MHz for plasma generation and heating. The usual pulse source for this work has consisted typically of a charged capacitor bank whose rapid discharge produces very large currents and peak power to the plasma load in a strongly damped, oscillatory discharge. In seeking a means for delivering a constant level rf burst to the plasma load, Weibel⁽¹⁾ took the approach illustrated in Figure 1. The circuit shown is essentially a lumped parameter transmission line made up in the usual manner from capacitors and inductors. However, unlike the passive artificial line, the capacitors are initially charged as indicated such that an approximate sinusoidal voltage profile is established. When the spark gap switches are simultaneously closed, the "frozen wave" is released in two oppositely propagating waves. The wave encountering the short circuit is totally reflected and phase-reversed so that, eventually, the load sees two complete rf cycles.

Weibel was successful in developing approximately 10 MW of power into a 4 ohm load at a frequency of 2 MHz. Later, Lietti developed a 10 cycle generator with power levels of 30 to 40 MW at frequencies of 1.5 to 2.0 MHz.

This earlier work on frozen wave generators can be summarized as follows:

- The generators were of the lumped element line type.
- Frequencies were in the 1 - 2 MHz regime.

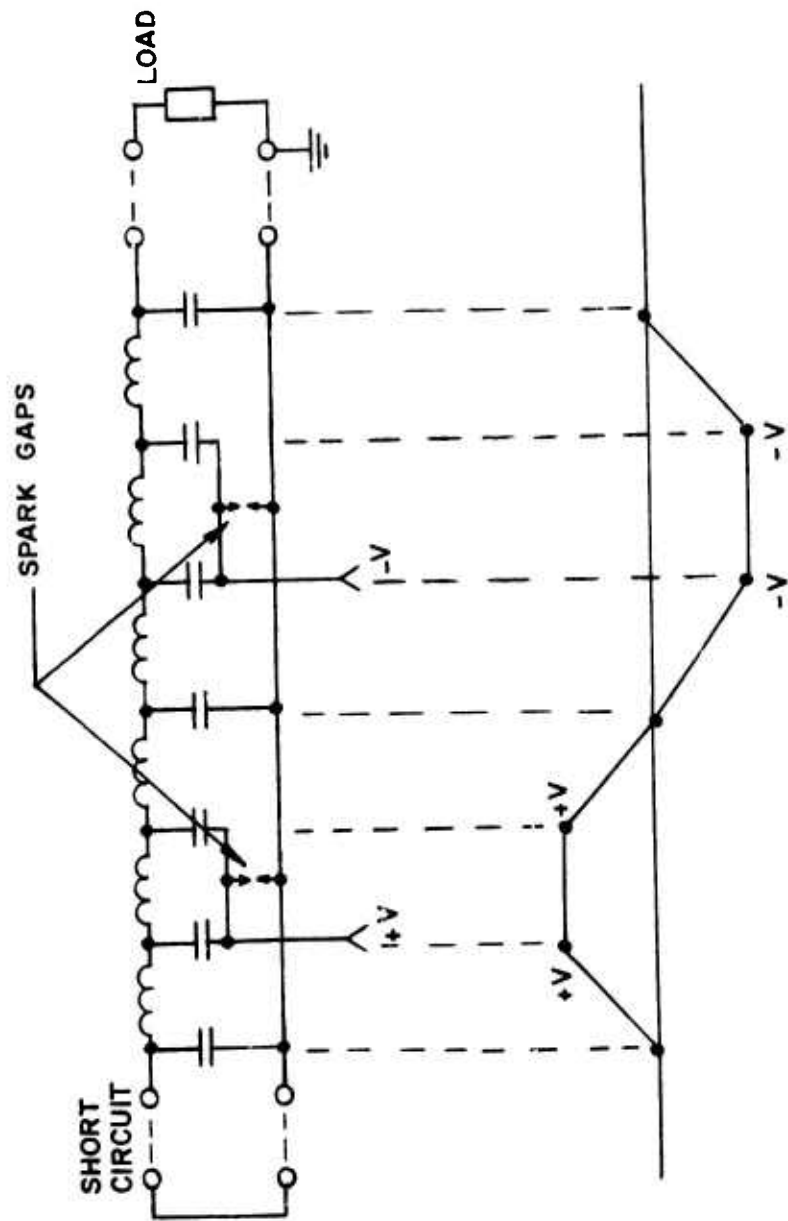


FIGURE 1. WEIBEL'S FROZEN WAVE GENERATOR

- Power levels of tens of megawatts were achieved, with no indication of any factor that would limit power levels of hundreds of megawatts.
- Experimental results generally confirmed the theory.
- Spark gap switches were seen as limiting generator capability.
- Efficiencies, overall, were very high.
- Sinusoidal waveforms, or at least trapezoidal approximates, were established as the frozen wave on the generator.

The switches used in these generators were triggered spark gap switches. It was pointed out by the authors of one of these papers⁽²⁾ that an inherent limitation to all lines employing spark gaps as switches exists; the firing time delay and jitter of the spark gaps have to fall within a time short compared with the period of oscillation. Hence, an upper frequency limit is imposed on lines switched by spark gaps. The implication is that this upper frequency limit is in the megahertz regime; in fact, there is such a limit, but it is in the hundreds of megahertz to gigahertz regime.

This gross underestimate of the frequency limit evidently came about because the authors were not aware of the advances taking place in the understanding of nanosecond and subnanosecond spark switch technology. In this time domain, spark switch properties become markedly different from those applicable to the microsecond domain.

It has been a general purpose of the investigation reported here to exploit the newer spark switch technology to attain efficient frozen wave generator performance in the gigahertz range.

2. THE BASIC MICROWAVE FROZEN WAVE GENERATOR

The prior work performed in the frozen wave generator art was accomplished in lumped parameter lines. Since concern in this investigation is with the lower end of the microwave spectrum, the transmission lines of interest are distributed parameter lines. For the purposes of this section, the specific type of transmission line need not be identified beyond requiring that

the lowest TEM mode of propagation is permitted. The specific means for charging the frozen wave, the switching means and associated triggering means are also left for later sections.

Reduced to its simplest form, the frozen wave generator produces two oppositely travelling square waves as illustrated in Figure 2. A basic transmission line configuration is shown in which adjacent, half-wavelength segments are charged initially to $+V_0$ and $-V_0$. The voltage waveform is then the square bipolar wave as shown. Upon the simultaneous closure of all the switches in the system, the frozen wave is released giving rise to two oppositely travelling waves having a peak-to-peak voltage of V_0 in matched impedance, Z .

In some applications, the inherent dual-direction wave generation of the frozen wave device may be of interest, e.g., in simple arrays. However, in most cases it will be of interest to achieve a single output. Figure 3 illustrates one means for designing a device where only a forward-going wave is produced. To accomplish this, a transmission line short is placed immediately adjacent to the last switch in the backward direction. The wave which propagates in this direction undergoes a 180° phase change and is reflected toward the forward direction to produce an uninterrupted wave having a duration, $2T$. The scheme whereby this wave is formed is illustrated in the figure.

Even though, ideally, the frozen wave generator is 100% efficient in producing a square wave, only 80% of the energy exists at the fundamental frequency. If it were possible to construct a perfect sine wave in the frozen state, its undistorted release would yield 100% conversion of the stored energy to the sine wave frequency. (NB - the energy stored, it must be realized, is only half the energy stored in the same amplitude square wave.)

A sine wave voltage distribution could be approximated by selectively charging the elements in a finely divided line as indicated in Figure 4 where five sub-segments are illustrated within each half wavelength of the stored wave. Upon switching, the positive and negative going "staircase" waveform is released, approximating a pure sine wave. Of course, more sub-elements improve the approximation.

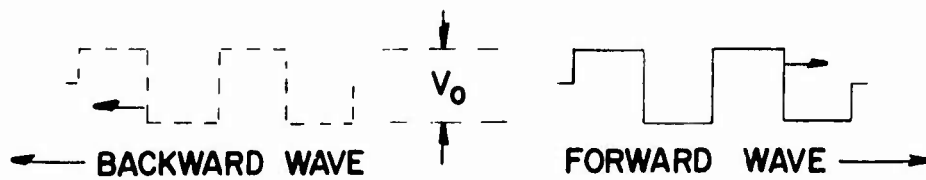
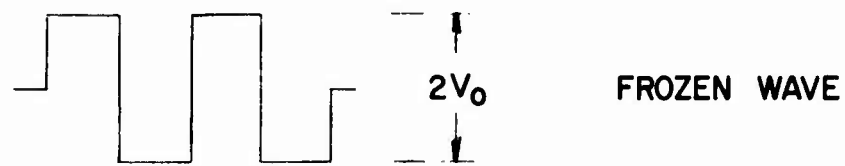
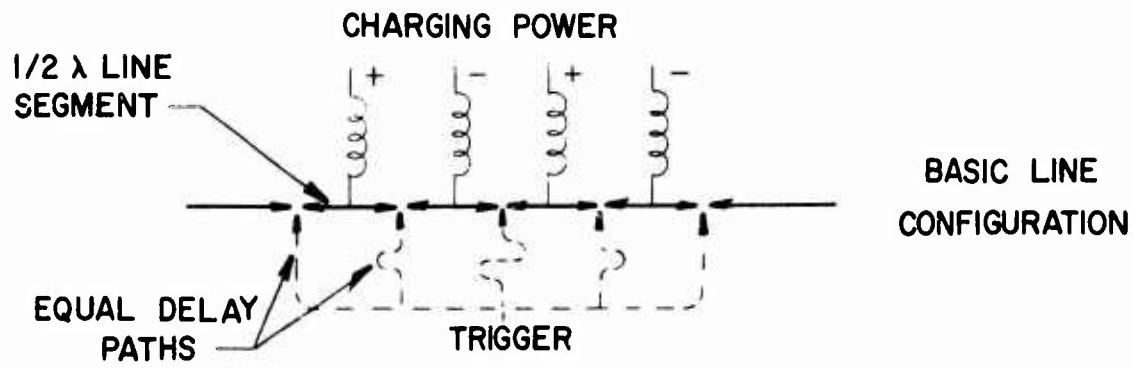


FIGURE 2.
BASIC FROZEN WAVE GENERATOR

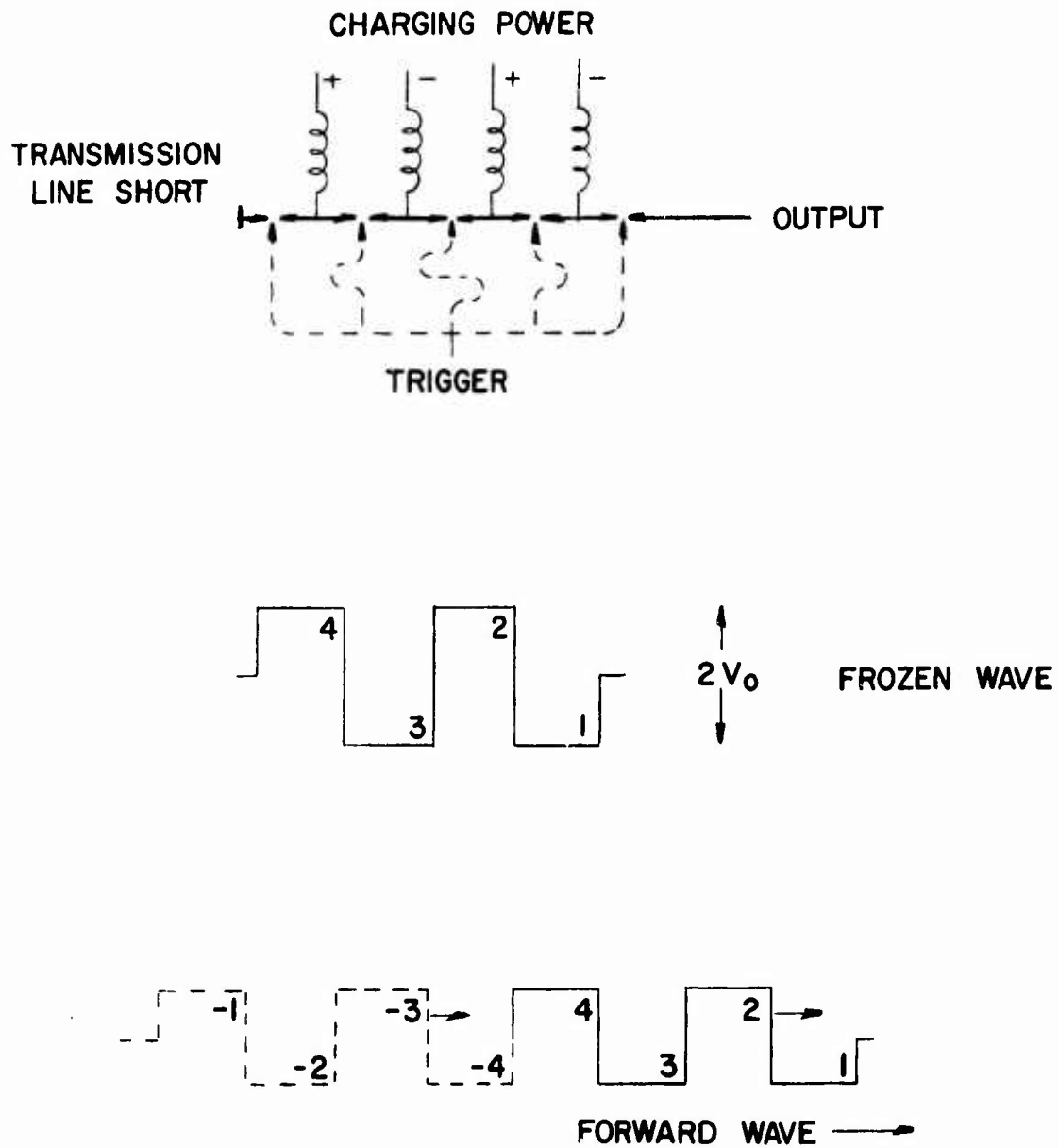
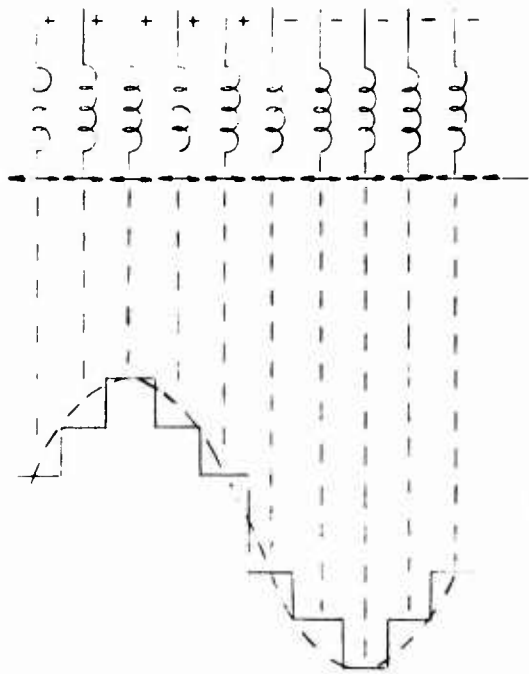
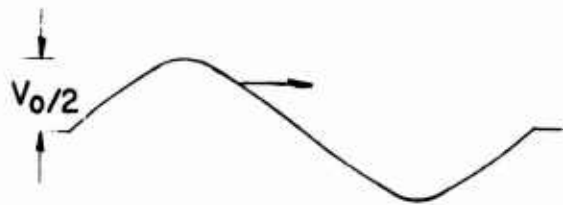


FIGURE 3.
 BASIC GENERATOR
 WITH SINGLE WAVE OUTPUT



FINELY DIVIDED
STORAGE LINE



FORWARD WAVE (APPROX)

FIGURE 4.
SINE WAVE APPROXIMATION

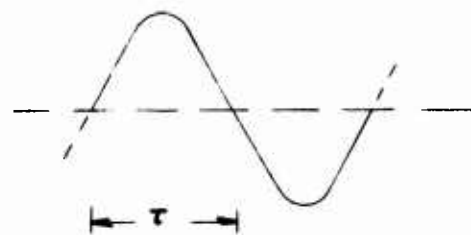
The benefits of setting up a frozen sine wave are offset in part, by the realization that, for comparable operating voltage, the square wave produces more power at the fundamental. Moreover, a number of other considerations also arise. For example:

- It seems likely that the switched waveform of the staircase type may produce widely dispersed high frequency harmonics if switch operation is near the ideal.
- If switch risetime is not small compared to sub-segment line length, a situation may be realized where the switch losses approach the energy stored, thus reducing the efficiency substantially.
- The problem of alternate polarity charging the segments of the simple form of frozen wave generator is not in itself trivial if done efficiently. Further subdivision may make practical charging schemes untenable.
- Alternative schemes performed on a dynamic basis, such as controlling switch risetime or grading line impedance, might offer better solutions.
- Of course, the extension of these "dynamic" control techniques is the narrow band or low pass filter.

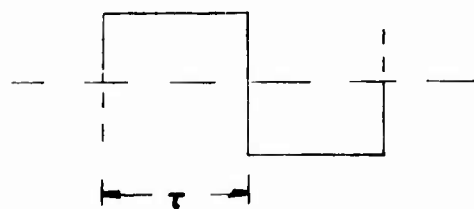
3. POWER SPECTRUM CONSIDERATION

Finite wave trains of three basic wave shapes have been analyzed to determine the resulting power spectrum characteristics. These include: the ideal sine wave, the ideal square wave and the trapezoidal wave having the parameters illustrated in Figure 5. The latter wave shape was picked to represent a first order approximation to the effects of finite switch risetime. Thus, even though approximate, the waveform is more realistic than either the sine or square wave.

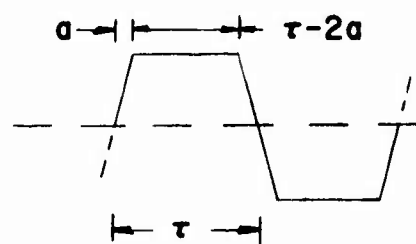
The half-period time τ is approximately 500 psec for frozen wave generators operating near 1.0 GHz. High voltage switch risetimes are typically in the 50 to 100 psec range. Therefore, in the numerical examples below we consider two representative cases: $a = 0.1\tau$ and $a = 0.3\tau$.



I. SINE WAVE



II. SQUARE WAVE



III. TRAPEZOIDAL WAVE

FIGURE 5.
ANALYZED WAVE SHAPES

The expressions for the power spectra (assuming unit time domain amplitude) for the three cases are as follows:

Case I - Sine Wave

$$|F(f)| = \frac{\tau}{2} \left[\frac{\sin(\pi\tau f - \pi/2)}{\pi\tau f - \pi/2} + \frac{\sin(\pi\tau f + \pi/2)}{\pi\tau f + \pi/2} \right] \frac{\sin(2\pi N\tau f)}{\cos(\pi\tau f)} \quad (1)$$

Case II - Square Wave

$$|F(f)| = \frac{\sin(\pi\tau f)}{\pi f} \frac{\sin(2\pi N\tau f)}{\cos(\pi\tau f)} \quad (2)$$

Case III - Trapezoidal Wave

$$|F(f)| = \frac{\sin[\pi(\tau - a)f]}{\pi^2 a f^2} \frac{\sin(\pi a f)}{\cos(\pi\tau f)} \frac{\sin(2\pi N\tau f)}{\cos(\pi\tau f)} \quad (3)$$

where: f is the rf frequency and N is the number of cycles in the wave packet.

Each power spectrum has a maximum of $f_1 = 1/2\tau$, the fundamental frequency. The square wave and trapezoidal wave have additional maxima at odd harmonics of the fundamental.

The location and magnitude of the spectral energy density maxima are given by:

Case I - Sine Wave

$$P(f_1) = 2N^2\tau^2 \quad (\text{fundamental only}) \quad (4)$$

Case II - Square Wave

$$P(f_r) = \frac{32N^2\tau^2}{r^2\pi^2}, \quad r = 1, 3, 5, \text{ etc.} \quad (5)$$

Case III - Trapezoidal Wave

$$P(f_r) = \frac{128N^2 r^2}{r^4 \pi^4 a^2} \sin^2 \left[\frac{r\pi}{2} \left(1 - \frac{a}{r}\right) \right] \sin^2 \left[\frac{r\pi a}{2r} \right] \quad (6)$$

$$r = 1, 3, 5, \text{ etc.}$$

Spectral maxima have a width equal to $1/N\tau$.

Table 1 presents a numerical summary of relative power density in the fundamental as well as the 3rd and 5th harmonics. As noted earlier, based on simple arguments, the square wave produces more power at the fundamental than does the sine wave assuming both time domain amplitudes are the same. Indeed, both trapezoidal waves illustrated also exhibit greater power at the fundamental. The idealized square wave is seen to possess substantial harmonic levels. However, for the trapezoidal wave with $a = 0.3\tau$, the harmonic maxima are nearly 30 dB down with respect to the fundamental. Further gains may be expected from intentional rounding of the voltage waveform.

TABLE 1. RELATIVE POWER SPECTRUM MAXIMA

	Power at f_1 (relative to Sine Wave)*	Power at f_3 (relative to f_1)	Power at f_5 (relative to f_1)
<u>Case I</u> Sine Wave	1.0	0	0
<u>Case II</u> Square Wave	1.6	1.1×10^{-1}	4.0×10^{-2}
<u>Case III</u> Trapezoidal Wave $a = 0.1\tau$	1.5	8.4×10^{-2}	1.9×10^{-2}
Trapezoidal Wave $a = 0.3\tau$	1.1	1.9×10^{-3}	2.4×10^{-3}

*all wave forms assumed
to have same time domain
amplitude

4. SWITCHING CONSIDERATIONS

The previous published work on the frozen wave generator was done at frequencies of only a few megahertz. These devices employed lumped parameter transmission lines and high voltage switches which had been within the state-of-the-art for several decades. The translation of this work to microwave frequencies introduces two basic requirements: (1) the replacement of lumped parameter by distributed parameter transmission lines, and (2) the utilization of triggerable, high voltage switches capable of closure times in the sub-nanosecond rather than sub-microsecond time domain. The first of these requirements presents no particular difficulty. In fact, the distributed parameter line is much simpler than the lumped parameter line. The second requirement, however, presents a difficult challenge in that very fast, precisely controlled, high power switches are required.

a. General Requirements

For the simplest form of generator in which a square wave, or somewhat more realistically, a trapezoidal wave is generated, the risetime should be about 100 psec or less for good performance at 1 GHz. More generally, the switching transient from open to closed state should meet the condition:

$$\text{risetime} \doteq 0.1/f \quad (7)$$

The jitter in switch closure must generally be less than the risetime, the precise value being dependent on phase coherency requirements. At L-Band, 1° of phase angle corresponds to about 3 psec of time displacement. Generally, the condition on jitter is:

$$\text{jitter} \doteq \frac{2.8 \times 10^{-3} \theta_m}{f} \quad (8)$$

where θ_m is the maximum tolerable phase shift between rf cycles. Typically, θ_m might be 5 to 10° , permitting a maximum jitter at L-Band of 15 to 30 psec.

While the above requirements are stringent, the situation becomes

worse if a further division of the frozen wave storage profile is attempted by subdividing the line segments. If the profiled wave is to emanate correctly, then the risetime must be small compared to the transit time in each sub-segment. Otherwise, the proper voltage or current waveform for each sub-segment is not released to its adjacent member, but rather, the stored energy is largely lost in the switching transient. For example, suppose each half-wave section of transmission line is subdivided n times. For the L-Band, the half-period time is about 500 psec. Then the switch risetime for each sub-segment must be substantially less than $500/n$ psec.

The voltage handling requirements of the frozen wave switch may be assessed by considering, initially, the idealized square wave generator. The idealized peak power released at the fundamental frequency is:

$$P = .80V_o^2/4Z \quad (9)$$

where the segmented line has been charged to $+V_o$ and $-V_o$. Then, in the square wave generator, the switches must sustain a potential difference of $2V_o$ where:

$$2V_o = 2(5ZP)^{1/2} \quad (10)$$

For $P = 1$ MW and $Z = 50$ ohms, the switch voltage holdoff is: $2V_o \doteq 30$ KV. Lowering the impedance will reduce this value, but for practical design this might produce, at best, a threefold reduction.

The use of subdivided segments can reduce the required voltage drop per switch approximately as V_o/n but in view of the above cited risetime constraint, n must generally be limited to small values.

The peak pulse current is given simply by:

$$I_o = (P/Z)^{1/2} \quad (11)$$

For $P = 1$ MW and $Z = 50$ ohms, $I_o \doteq 150$ amperes. Lowering the impedance to

reduce voltage requirements accordingly increases the current requirements.

There are, of course, additional requirements on the switches used in the frozen wave generator. For example, the series resistance R must be kept to small values such that $I_0^2 R$ is small compared with P . Also, in order to achieve the risetime requirement described by expression (7), the self-inductance must be small as indicated by the relationship:

$$\text{risetime} \doteq \frac{2L}{Z} \doteq \frac{0.1}{f} \quad (12)$$

Thus, for L-Band, L must be of the order of one nanohenry. Both L and R are functions of time in any fast-acting switch.

b. Spark Gap Switching

It is not an unexpected result that spark gap switch technique appears to offer the method most suitable for meeting the above requirements. Firstly, virtually all of the previous technology associated with high power Hertzian generators turned, for good reasons, to the use of spark gap switches. Secondly, the specific requirements stated above for voltage and current handling together with risetime and jitter are descriptive of modern achievable spark switch parameters.

The background work performed by Weibel⁽¹⁾ and Lietti⁽²⁾ on low frequency versions of the frozen wave generator utilized a spark gap technology which was known in their field of endeavor (plasma research) for sometime. The limitations that these investigators saw in spark gap switching stemmed from well known loss mechanisms operative on a microsecond time scale, the lack of any fast trigger control scheme and the absence in their field of any switch with nanosecond closure properties.

Many of the time constants associated with the plasma properties of the high density arc formed when the spark switch closes are of the order of microseconds. This would include recombination, hydrodynamic phenomena, thermal relaxation, etc. Thus, it is not surprising that the arc resistance losses are high when current reverses on this same time scale. In the nano-

second domain, the spark switch makes a rapid transition to the conducting state and passes bipolar waves readily with small loss. In microwave Hertzian generators, the effects of the above time constants are felt only long after the desired switch function is completed.

Much of the past success achieved in attaining risetime and trigger jitter characteristics, such as are required in the microwave version of the frozen wave generator, derives from an exploitation of overvolted spark conditions. Such conditions exist only on a nanosecond or sub-nanosecond time scale where the time constants associated with statistical lag⁽³⁾ (field emission) and formative times⁽⁴⁾ are determinants of the closure properties. When voltage stresses are applied on these time scales, closure times can be made very short, e.g., in the range between 10 and 100 psec. Similarly, the highly overvolted spark switch may be triggered by UV irradiation (producing photoelectrons) with extremely small jitter⁽³⁾.

With respect to voltage handling versus switching speed, the spark switch is the converse of the semiconductor switch. That is, the greater the operating voltage, the easier it becomes to accomplish fast risetime, low jitter and low loss switch closure.

c. Fast UV Triggering

The development and utilization of ultra-fast spark gap switch technology has been evidenced by the successful operation of the Travatron^(5, 6, 7), the Imp Generator^(8, 9) and, more recently, a high power X-Band generator, the Cavatron^(10, 11). All of these devices depend upon attainment of voltage, current, risetime, low loss and low inductance properties similar to those required in the microwave frozen wave generator. The additional requirement, unique to the frozen wave generator, is for a means for simultaneously closing a number of switches with low inter-switch jitter.

The basic ingredient for fast closure of a spark gap is high overvoltage as noted above. The two components of lag time which can then be manipulated are statistical lag and formative lag. A third fast process, UV

induced photoemission, can be added for control (trigger) purposes. The three processes together with generalized parameter dependencies may be summarized as follows:

Statistical Lag: In the absence of any other source of electrons, the statistical lag is inversely proportional to the electron field emission rate. Thus, the statistical lag is determined primarily by the local electric field at the cathode and by the electrode material. By varying these parameters in fast, highly overvolted switches, statistical lag components ranging from approximately 50 psec to 10 nsec have been achieved.⁽³⁾

Formative Lag: The formative lag component determines the rate at which the gap impedance collapses by electron impact ionization resulting in breakdown. It is controlled by the average electric field, the gas species present and the gas pressure.⁽⁴⁾ The formative time can range from 10 psec to many nsec.

Photoemission: The photoelectric effect, discovered by Hertz in 1887 while experimenting with "Hertz" generators⁽¹²⁾, may be used to produce initial electrons to trigger the above formative processes. The number and energy of electrons produced depends upon the intensity and wavelength of the incident optical radiation which, for most cathode materials, must lie in the ultra-violet to overcome the surface work function. Experiments have demonstrated trigger capability using UV pulse sources having jitter near 25 psec in overvolted gaps.⁽³⁾

Taken together, the three processes can provide a means for obtaining all of the switch requirements cited by designing the switch to sustain a desired impressed voltage without breakdown for a period of several nanoseconds using the appropriate parameters governing statistical lag. Then, if a fast rising UV pulse is applied to the cathode during this statistical period, the breakdown process can be initiated by the first few incident photons. It remains to choose an E/r ratio (see Reference 4) such that the rate of closure is as fast as desired.

An obvious and convenient UV pulse source for triggering a spark gap switch is another spark gap. The rapidly formed, high temperature plasma in such a gap is a rich source of UV and its rate of rise is comparable to the formative time.

Following this approach, previous experimentation was highly successful in time locking one overvolted spark switch with the closing of another similar gap. Trigger jitter was near the 25 psec time resolution limit of the apparatus used in those observations. The experiments were extended to obtain an estimate of the spectrum interval most important in the light coupling. This was determined to lie in the 2000 - 3000 A° range.

It is a straightforward extension of this technique to arrange for one "master" spark UV source to illuminate and therefore trigger a large number of "slaves." The design approach for the frozen wave generator investigated in this study is based on this extension. The concept has proven successful in tests of breadboard generators to be discussed in later sections.

5. DESIGN CONFIGURATIONS

The basic generators illustrated above in Figures 2 and 3 are representations of linear devices. That is, the transmission line is arranged of straight, in-line segments. The extension of this has several deficiencies when applied to practical generators. One of these is the fact that, as the desired pulse length increases, so does the physical length of the device. Eventually, one can visualize unwieldy form factors.

A more important limitation arises in connection with the need to provide simultaneous triggers for each switch. This requirement dictates that the propagation paths from any master control signal be made identical to within a small fraction of the rf wavelength.

a. Circular Disc

A configuration which surmounts both problems is illustrated in Figure 6. Here the segmented transmission line is layed out in a circle to

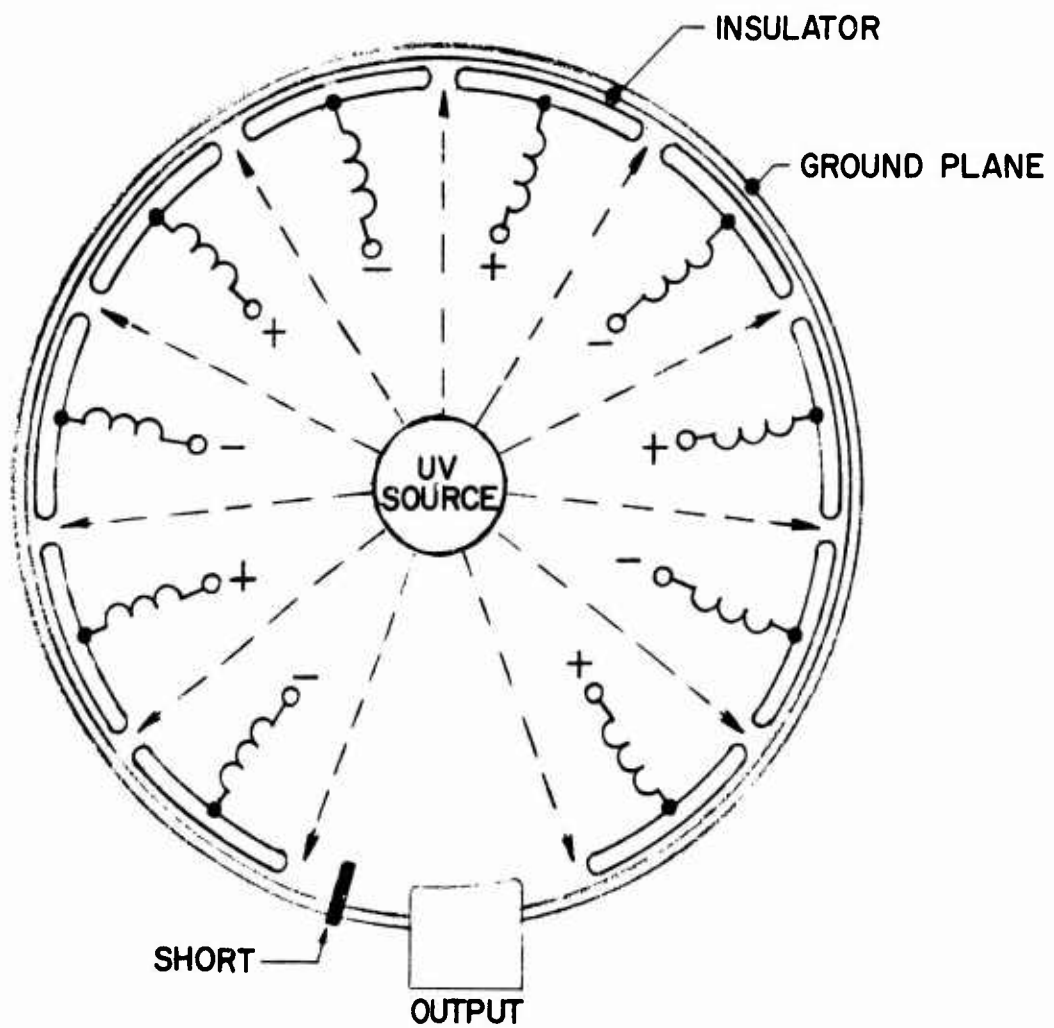


FIGURE 6.
A CURVED STRIPLINE GENERATOR

surround the trigger signal source. All switches in the system are then equidistant along straight line paths from the trigger. The geometry is particularly suitable for the case illustrated where spark switches are triggered in their overvolted state by a single UV pulse source. The flat disc package geometry resulting from this basic configuration offers a variety of interesting avenues for design. For example, it lends itself to scaling to both higher and lower frequencies. Also, it suggests "stacking" schemes for higher power output which take advantage of the form factor as well as the simple, single point trigger method.

In the arrangement of Figure 6, it is visualized that the frozen wave segments are arranged around the inner wall of an annular ring of appropriate dielectric. The outer conducting shell forms a curved ground surface. A ten-segment generator is shown with eleven switches. A reflecting short is provided to yield forward wave output as described above in connection with Figure 3. Such a generator would then produce 10 cycles of rf.

A simplified version of this generator was investigated in the experimental effort to gain preliminary assessment of problems associated with: 1) simultaneous UV triggering, 2) uniformity (or lack of uniformity) of the transmission line, and 3) reflection of the backward propagating wave.

b. Folded Line-Disc Geometry

Another interesting version of the disc generator possessing several attractive features is illustrated in Figure 7. Here, the stripline segments of opposite charge polarity are arranged on alternate sides of a central ground plane. In order to achieve a compact layout and to locate the spark switches very close to the UV trigger, the half-wave segments are folded as indicated. The spark switches run vertically between upper and lower segments and are arranged in a circle very near the central UV trigger source. Pulse power ($-V_0$ for the upper plane and $+V_0$ for the lower plane) is fed through the inductive charge paths as indicated. In all, five upper and five lower plane segments are represented with a transmission line short (not shown) to provide forward wave propagation.

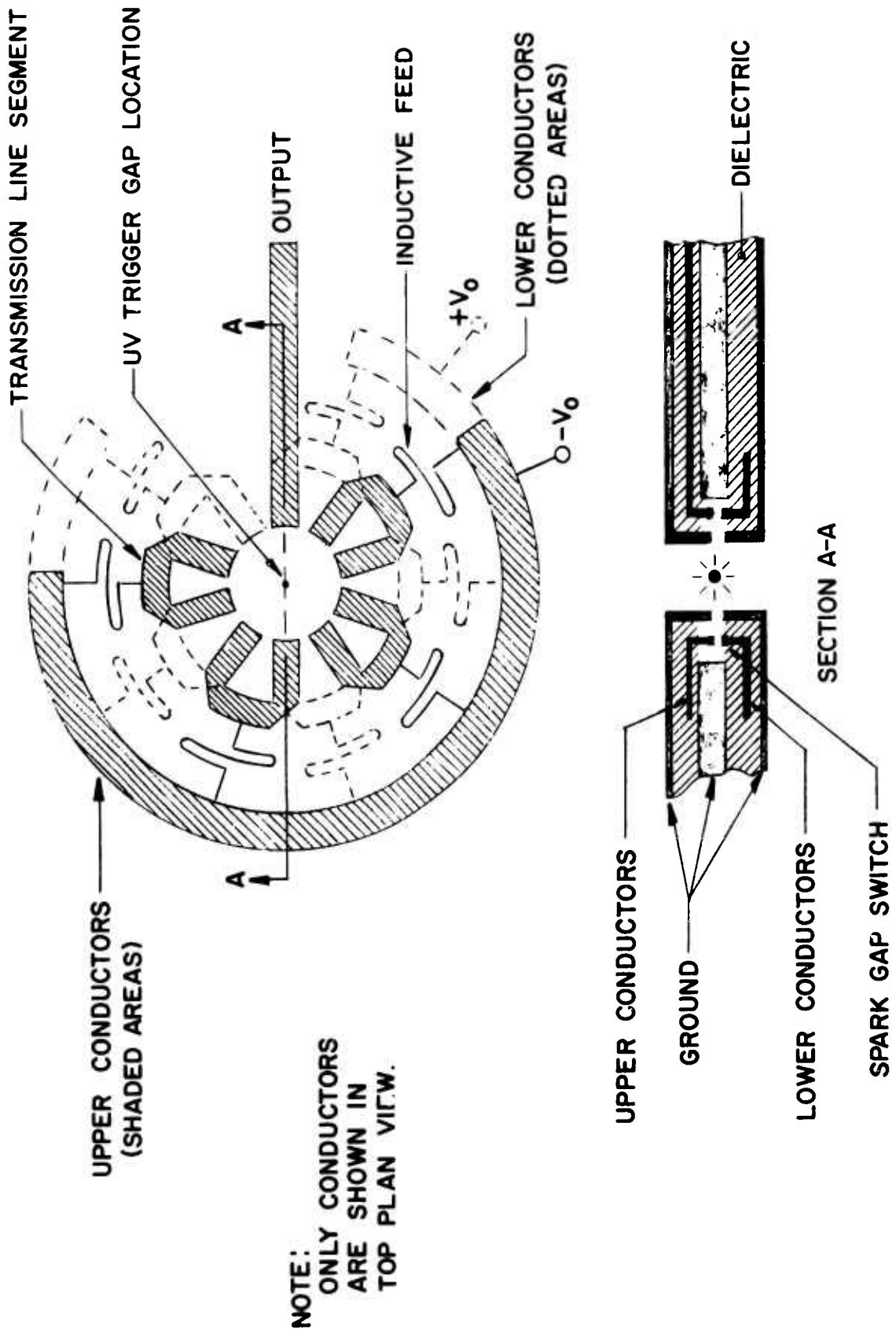


FIGURE 7. SCHEMATIC OF A FOLDED LINE GENERATOR

The outstanding features of this schematic design are: (1) its compactness, (2) its inherent close coupling to the UV trigger and, (3) its high voltage capability. The latter stems largely from the fact that adjacent segments in one plane are all at the same pulse charge potential. Thus, surface creepage and corona problems are minimized.

A folded line frozen wave generator designed to operate at 1.3 GHz was built as part of the program effort. It was a ten segment device; the transmission line design impedance was 50 ohms. A detailed discussion of the design and test results is given in a later section.

c. Coaxial Cable Designs

At frequencies substantially below 1 GHz, the segment length becomes sufficiently large that flexible coaxial cable can be utilized. A design approach employed successfully in this program consisted of coaxial cable segments arranged so that their switched ends were clustered at the center of the structure. The coplanar spark switches then describe a circle whose diameter can be made quite small to enhance UV coupling. The program experience, detailed in a later section, suggests an upper frequency limit near 500 MHz for generators employing coaxial lines.

6. INPUT REQUIREMENTS

As reviewed above, the frozen wave generator operates on the principle that a "dc" voltage profile is established and subsequently released by synchronous switching. Actually, the frozen wave profile must be reestablished at a rate determined by the desired PRF of the device and, of critical importance to the switching method described above, the voltage must be developed very rapidly to bring about fast overvoltage conditions. The required time scale for charging is then in the nanosecond range. The central problem regarding the input is one of achieving efficient and rapid development of the frozen wave profile.

To assess the problems associated with pulse charging, it is instructive to consider the circuit parameters involved. A megawatt output pulse in a 50

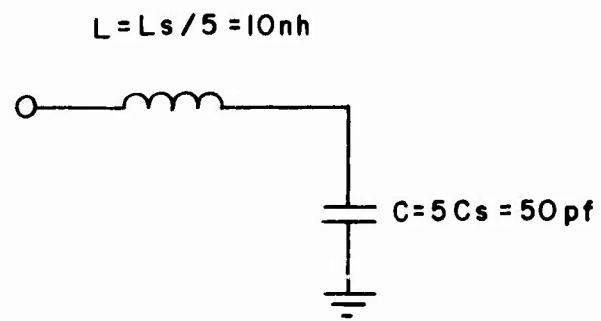
ohm system requires an initial frozen square wave profile with $\pm V_0 \cong 16$ KV. With the exception of the first and last spark switch in the generator, the maximum potential drop across each switch is then 32 KV. A ten-cycle generator, with forward wave output only (see Figure 3), will have 5 positive and 5 negative, half-wave segments. For an L-Band generator in 50 ohms, the segments will have a capacity C_s per segment of approximately 10 pf. Therefore, the positive and negative input sources must each supply a capacity load of about 50 pf.

An additional requirement placed on the input circuitry is a means for isolating the generated rf in the frozen wave generator from the input feed. From efficiency considerations, an obvious choice is inductive isolation where the value of inductance L_s feeding each segment is chosen to present a large impedance compared to 50 ohms. In addition, the inductor must be located very near the segment to be charged and its self-resonant frequency must be well above the generator frequency. To satisfy the first requirement, an inductance value on the order of 100 nh is appropriate.

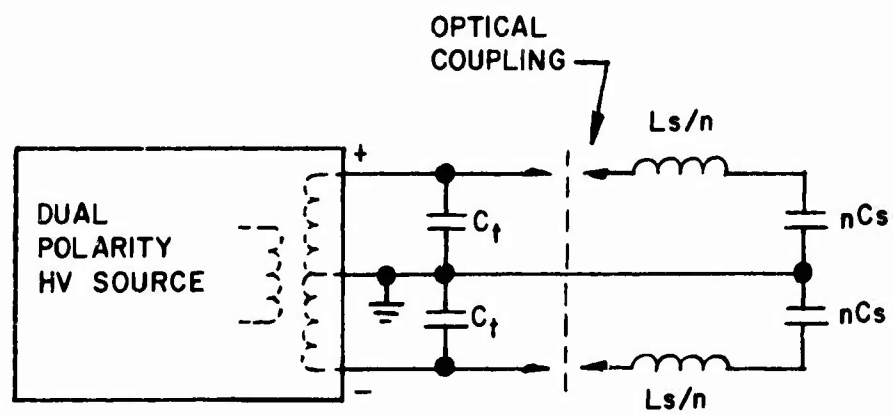
Following this design approach, the input pulser for each polarity must feed the simple series resonant circuit depicted in Figure 8(a). The resonant frequency of the equivalent input circuit is near 225 MHz which is in good accord with the charging rates needed.

Figure 8(b) presents an implementation scheme used in the investigation to provide simultaneous charging of positive and negative segments in the generator. In this scheme, tandem capacitances C_t are charged from a common pulse transformer to opposite polarity potentials. Following this relatively slow charging process (microseconds), the stored energy is switched in synchronism through the charging inductors, thereby transferring the stored charge to the generator segment capacitance. Synchronism on a nanosecond scale is accomplished by mutual UV coupling of the two transfer switches.

The simple resonant transfer circuit is theoretically a highly efficient one when the transfer capacitance C_t just matches the combined segment capacitance. If C_t is large, the usual resonant charging conditions are met such



(a) EQUIVALENT CIRCUIT FOR 50 OHM SYSTEM



(b) A DUAL POLARITY PULSE CHARGING SCHEME

FIGURE 8. INPUT PULSE CHARGING CIRCUITS

that voltage doubling occurs, but the efficiency is degraded.⁽⁷⁾

A number of difficult problems arise in implementing resonant charging schemes of this type, which are directly related to the needed circuit parameters. For example, the small value of C_t required for efficient energy transfer makes C_t very difficult to charge efficiently in the first place. One key problem in this regard is due to the appreciable capacitance of the high voltage secondary winding of the pulse transformer. Resistive charging, even though it is less than 50% efficient, offers a viable alternative.

For the lumped element analysis of the above circuit to hold, actual physical spacing is of key importance. In view of the nanosecond time scale of interest the entire circuit must have dimensions of at most a few inches. This compactness requirement, in conjunction with the need for dual polarity, high voltages, presents an additional measure of difficulty.

The previous work referenced above in attaining synchronism of over-volted spark switches by UV coupling was performed experimentally with resistive damping of the applied potentials. Resistive charging of this type has the advantage of providing smooth increases in the potential drop across such switches, thus making their subsequent triggering more reliable. An alternative approach involves the use of relatively low frequency resonant charging. Efficiency and degree of overvoltage are trade-off considerations in either case. The next section reports an effort conducted in this program to obtain data and better understanding of the processes involved.

SECTION III

SPARK GAP PHENOMENA AND POWER LIMITS

To be feasible at microwave frequencies, the frozen wave generator must incorporate switches capable of withstanding high voltages for a time on the order of nanoseconds. Following this hold-off period, the switches must close on command with closure times in the subnanosecond region. In the closed state, the switches must exhibit low series impedance such that the rf circuit is established with little mismatch or loss.

As reviewed in the previous section, the overvolted, UV triggered spark gap appears to offer considerable promise in meeting these requirements. Supporting data derives from previous experimentation⁽³⁾ in which two spark gap switches, charged via a damping resistor, were successfully synchronized through mutual UV coupling. In those tests, it was determined that trigger jitter as low as 25 picoseconds could be attained while working in the 20 KV range with overvoltage periods near one nanosecond.

This earlier study requires extension in three key areas when applied to the frozen wave generator operating at microwave frequencies. First, the UV triggering process, whether it is accomplished by mutual illumination or by a master UV pulse source, must be extended to several switches. Secondly, the lag period prior to command triggering must be extended to several nanoseconds to ensure that charging is accomplished on a time scale considerably longer than one rf period. Finally, the power input to the generator must be performed with dual polarity charging voltages applied through circuits or networks generally more efficient than charging resistors.

In order to gain useful insights concerning these areas, an experimental investigation was performed to expand the data base regarding optically coupled spark gaps. In addition, a theoretical treatment of spark gap lag as affected by the rise time of the applied pulse was carried out and experimentally verified. Finally, a theoretical estimate of frozen wave generator power limits was formulated. The findings are reported in the following paragraphs.

1. UV TRIGGERING INVESTIGATIONS

The delay and UV triggering statistics of two optically coupled coaxial line spark gaps were explored using the experimental arrangement shown in Figure 9. Whereas in the earlier study using a similar arrangement, identical spark gaps were charged resistively, the investigation described here employs resonant charging technique and allows for unequal charge voltages, gap spacings and independent control of rise time.

In the experiment illustrated in Figure 9, two short coaxial lines are resonantly charged by the discharge of the transfer capacitance C_t through spark gap g_o and the inductances L_1 and L_2 . The two coaxial spark gaps g_1 and g_2 under study then close, launching a pulse into a matched, terminated line as indicated. Optical coupling is provided along the variable air path of length d . Voltage waveform probes are located at either side of the two gaps. The monitors at the input sides of g_1 and g_2 allow for viewing of the waveform impressed on each gap. The output monitors are used to provide data concerning the relative closure times. The probe signals are simply added and fed to the input of the oscilloscope (Tektronix 519). The signal from g_2 is delayed relative to that from g_1 by a fixed 6.2 ns. In operation the gaps g_1 and g_2 are always adjusted such that g_1 is the control or trigger gap and g_2 is the slave. Thus two distinct pulses appear on the oscilloscope consisting of the pulse launched by g_1 , which also triggers the sweep, and the pulse from g_2 which arrives with a delay of 6.2 ns plus the lag time of g_2 .

The experimentation was aimed at the development of the statistics regarding the lag time and jitter between the closure of g_1 and g_2 . Typically, about 25 trials were run for each experimental situation. The data were then analyzed as indicated in Figure 10 which represents the UV triggering statistics for three optical paths. In this case, g_1 and g_2 were simultaneously charged to 25 KV with an input rise time of approximately 5 ns. The gap spacing of g_1 was .015 in with g_2 set at .025 in.

For each value of d indicated in Figure 10, the fraction of trials N/N_o having a lag greater than τ is plotted against τ . The average value $\bar{\tau}$ and

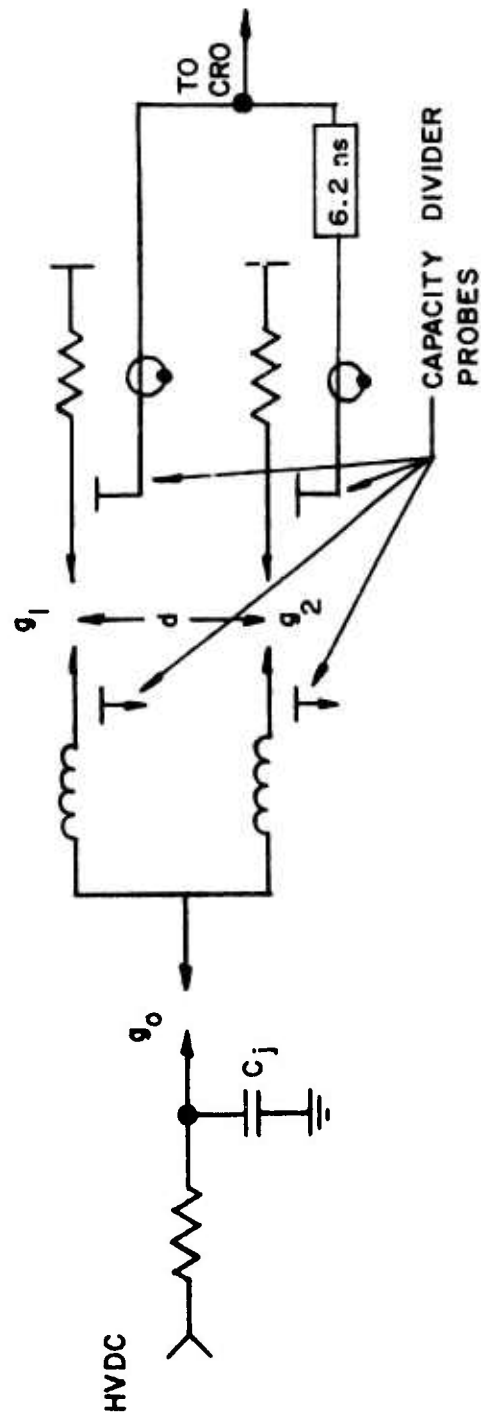


FIGURE 9. UV TRIGGERING EXPERIMENT

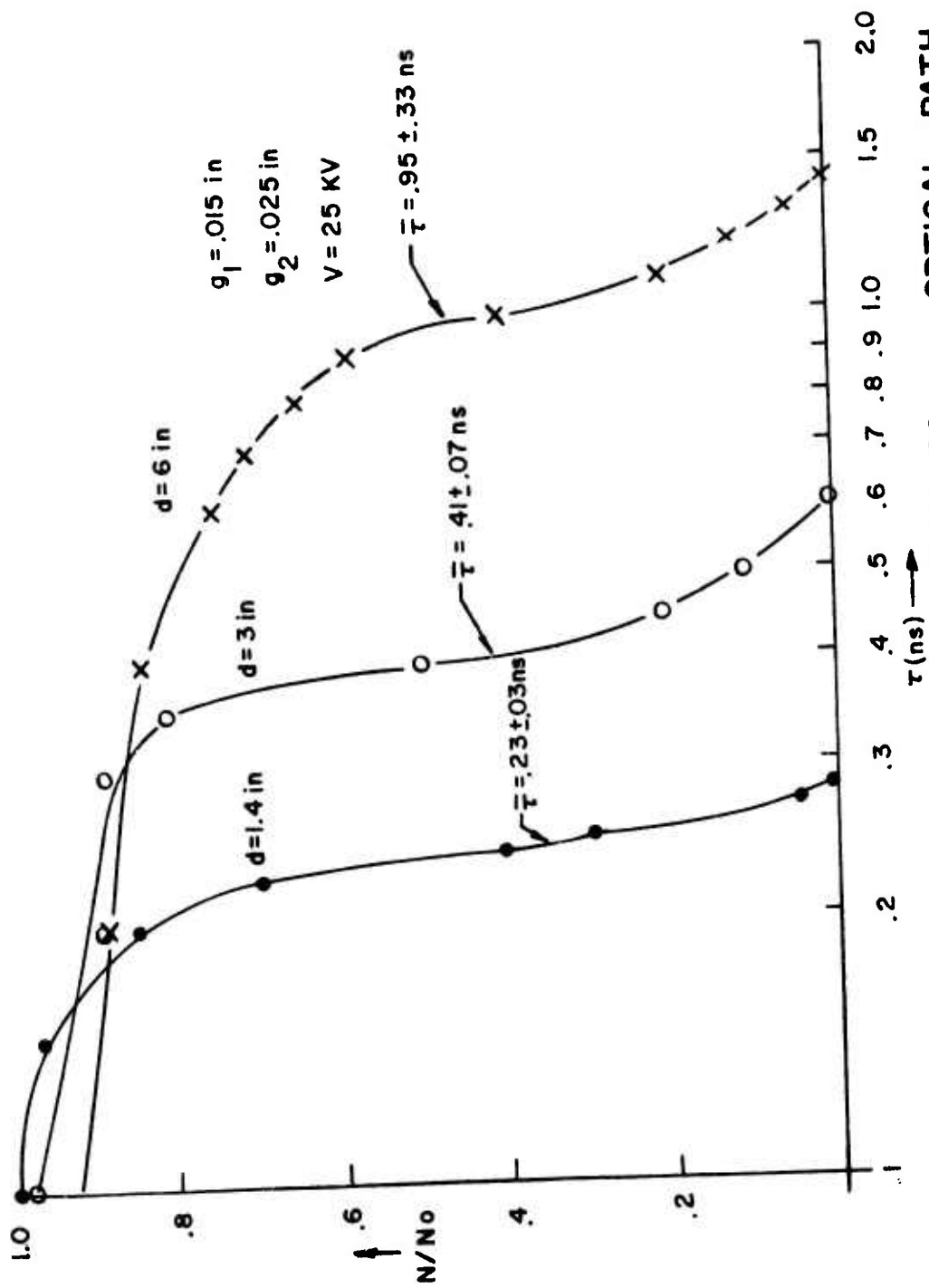


FIGURE 10. UV TRIGGERING STATISTICS vs. OPTICAL PATH

RMS deviation or average jitter were also computed and are indicated in the figure. The average lag time and jitter is shown to be a strong function of the optical path length or, equivalently, of the UV illumination reaching gap g_2 from g_1 .

Figure 11 shows similar data for various field strengths. The curve exhibiting the smallest lag and jitter was replotted from Figure 10. The other two curves were obtained with the same maximum field strength of 240 KV/cm, obtained by charging both g_1 and g_2 to 15 KV and 12 KV with g_2 set at .025 in and .020 in, respectively. In all cases, $g_1 = .015$ in and $d = 1.4$ in. It may be seen that the lag and jitter are strongly dependent upon field strength in g_2 but depend only weakly upon the actual gap space.

The results shown in Figure 12 were obtained by increasing the value of L_2 so that the potential applied to g_2 rises more slowly. In addition, a delay was imposed between L_1 and g_1 to provide a delayed fast rising pulse to g_1 . By these means, g_2 was triggered at a lower voltage level as compared to the previous cases. The data in Figure 12 were for the case where the field strength at g_2 was only 45 KV/cm and 60 KV/cm. Even at these low overvoltage levels, the jitter is in the subnanosecond range and, as before, there is a very strong dependence of jitter on the optical path length.

The above results confirm the conclusion of previous work regarding the ability to close two overvolted spark gaps with very high reliability by means of mutual UV coupling. Moreover, the results obtained in this study show that UV coupling is effective in synchronizing dissimilar gaps even when relatively small overvoltage ratios exist (e.g., 1.5 to 2.0) in the triggered switch. However, in this latter case the jitter would be unacceptable for the microwave frozen wave generator, as revealed by inspection of Figure 12. Referring to the curve shown having a mean lag time of 1.4 ns and a jitter of 0.5 ns, it is seen that 10% of the trials had a lag time less than 0.7 ns, while another 10% had lags greater than 2.0 ns. In constructing a frozen wave generator possessing, say, 10 switches with these characteristics, the probability of one switch "misfiring" is very high. Such an event is not acceptable in the frozen wave generator. The curves shown in Figure 11, for example, exhibit triggered

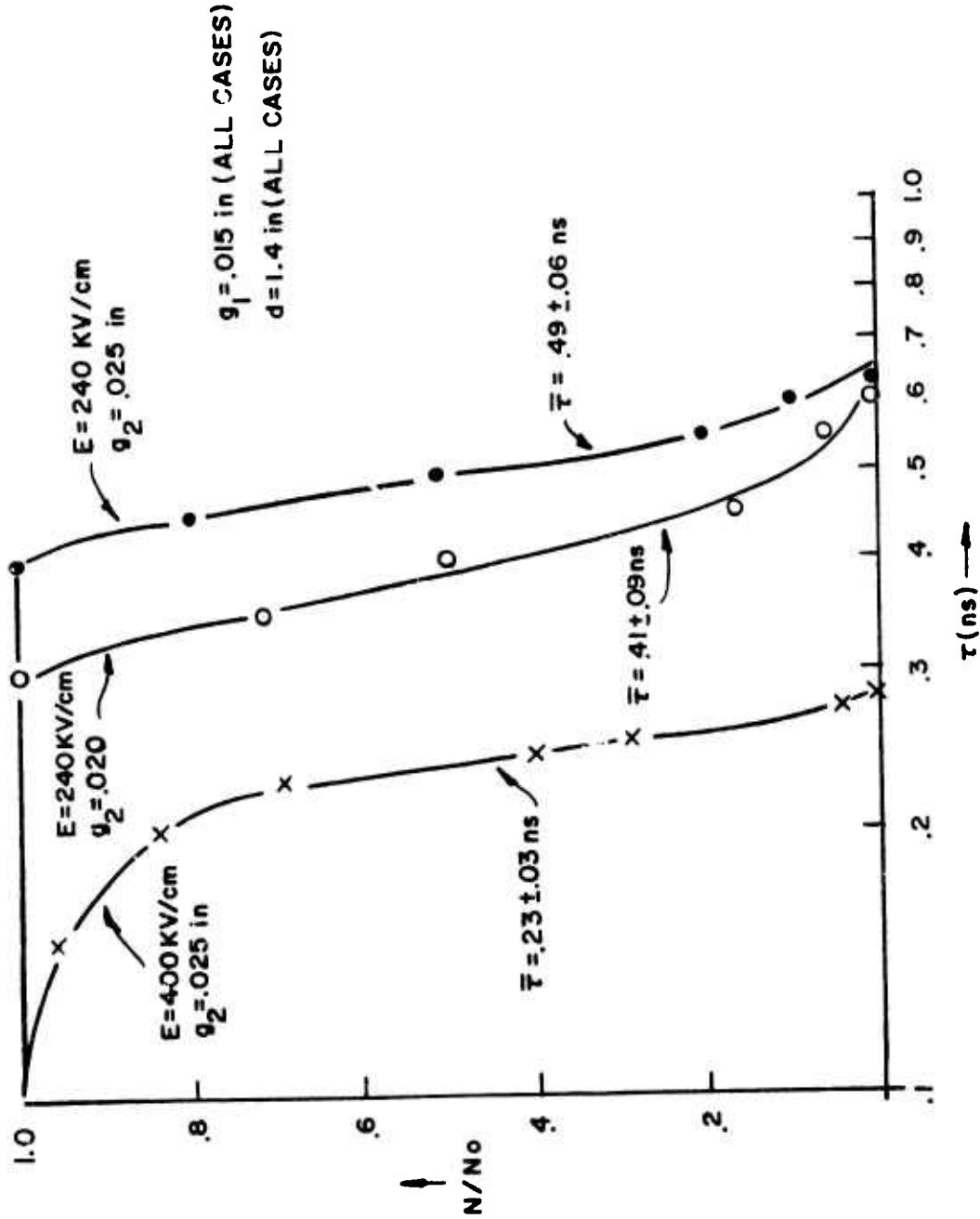


FIGURE II. UV TRIGGERING STATISTICS vs. FIELD STRENGTH

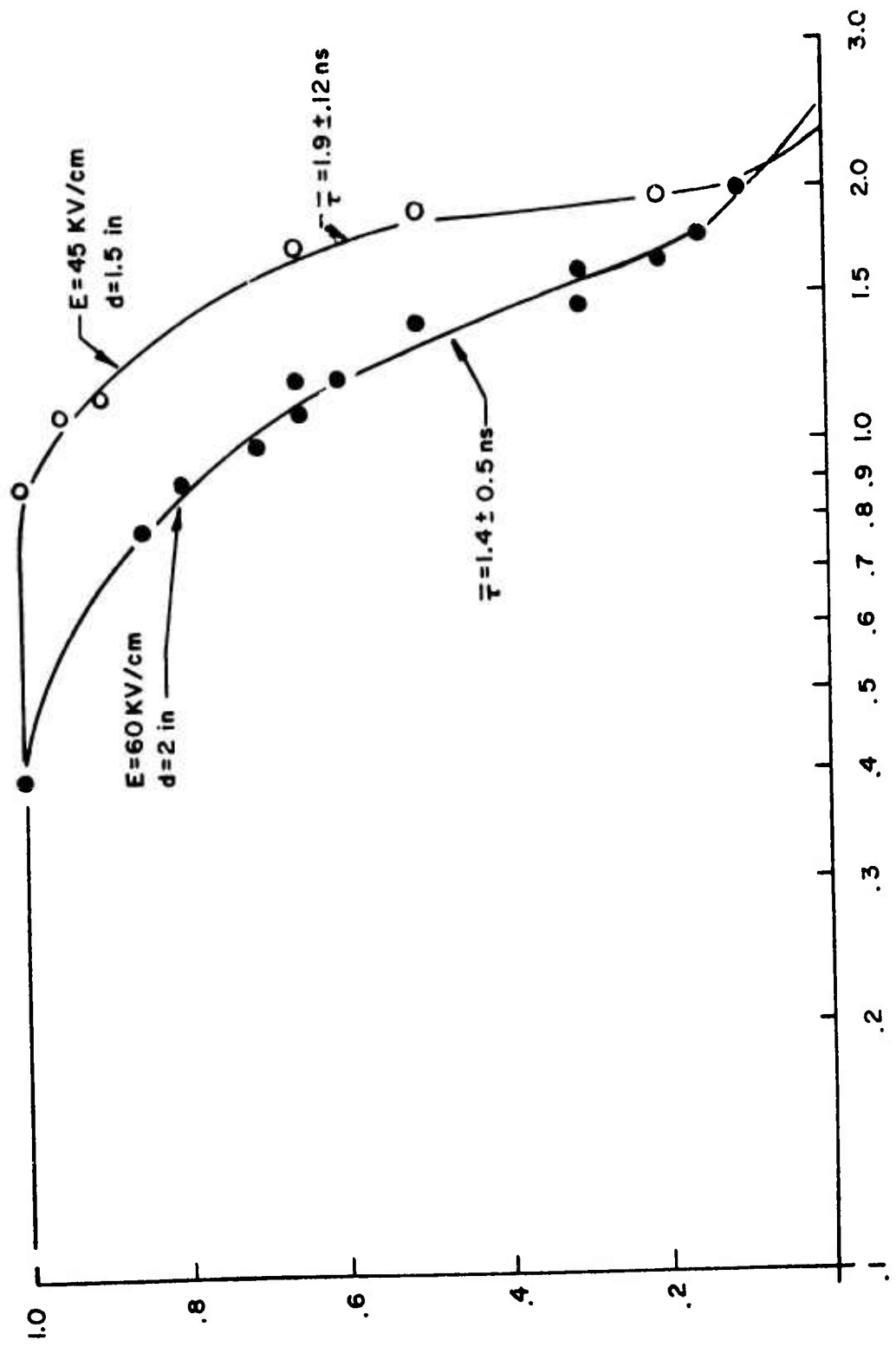


FIGURE 12. UV TRIGGERING STATISTICS

switch characteristics which do not present the above difficulty since, in the worst case, the total spread in closure time is less than 0.3 ns. Here, however, very high overvoltage ratios are required (e.g., 10:1) and the question arises as to the ability of the switch to hold off the high overvoltage condition for periods of several nanoseconds. A related question also arises as to the effects of the rise time of the charging pulse on the total lag period. Some insights are provided in the following.

2. SPARK GAP LAG FOR TIME DEPENDENT OVERVOLTAGE

The statistical lag time in an overvolted spark gap is generally defined as that component of the lag time which is dependent upon the appearance of electrons following the application of a voltage step. As cited previously, the particular electron producing process of interest here is field emission. In the frozen wave generator, the electric fields causing field emission must be applied relatively slowly leading to an interrelationship between the rise time, the total lag time and the breakdown voltage. To form an estimate of the effects of finite rise time, an approximate analysis has been conducted which is based, in part, upon prior empirical results for rapidly overvolted gaps.

In the presence of a high electric field E , the field emission current density j is expected to obey the Fowler-Nordheim relationship:

$$j = AE^2 \exp(-B/E) \quad (13)$$

where A and B are constants of the material. In the analytical model employed here, it is visualized that a critical number σ_c of electrons per unit area must be emitted to precipitate breakdown by subsequent processes such as collisional ionization. The critical charge density is then defined by:

$$\sigma_c = \int_0^{t_s} j \, dt \quad (14)$$

where t_s is the statistical lag time. When the applied field is applied as a step function, the current density is constant in time and the integration yields

$$t_s = \sigma_c / j = \sigma_c / A \cdot E^{-2} \exp(B/E) \quad (15)$$

Previous investigation⁽³⁾ of statistical lag in rapidly overvolted gaps showed a field dependence resembling that of equation (15) provided that the constants were chosen such that $B = 870$ and $\sigma_c / A = 7000$ where t_s is expressed in nanoseconds and E is in kilovolts/cm. These values applied to a spark gap configuration and a material very similar to that used in the frozen wave generator.

To calculate the statistical lag time as modified by the time dependence of E , equations (13) and (14) may be used with the known constants. The time dependence of the field must be known explicitly before integration can be carried out and will, of course, depend upon the experimental set-up. It has been assumed for calculational purposes here to have the form:

$$E(t) = E_m [1 - \exp(-t/\tau)] \quad (16)$$

This exponentially rising function is chosen because it corresponds to a real physical situation, i.e., resistive charging, and is readily handled in computations since it is monotonic. The integral evaluated to determine t_s is then

$$\int_0^{t_s} E^2(t) \exp[-870/E(t)] = \sigma_c / A = 7000 \quad (17)$$

with $E(t)$ given by (16).

Equation (17) was integrated numerically with the upper limit of integration as a parameter. The value of t_s which satisfied (17) was then printed out and the corresponding value of E_B was determined from (16) where E_B is the breakdown value of E .

Table 2 summarizes the results for different values of the parameters E_m and τ in equation (16). The data are further illustrated graphically in Figure 13. The most important feature observed is that the breakdown field strength of the gap is lessened as the rise time of the applied field is increased. As seen in

STATISTICAL LAG PROPERTIES FOR VARIOUS E(t)

TABLE 2

	τ (ns)	E_B (KV/cm)	t_s (ns)
$E_m = 200$ KV/cm	1	200	17
	5	199	27
	10	195	38
	20	189	58

$E_m = 300$ KV/cm	1	292	3.7
	5	261	10
	10	244	17
	20	227	29

$E_m = 400$ KV/cm	1	351	2.1
	5	296	6.8
	10	269	10
	20	249	20

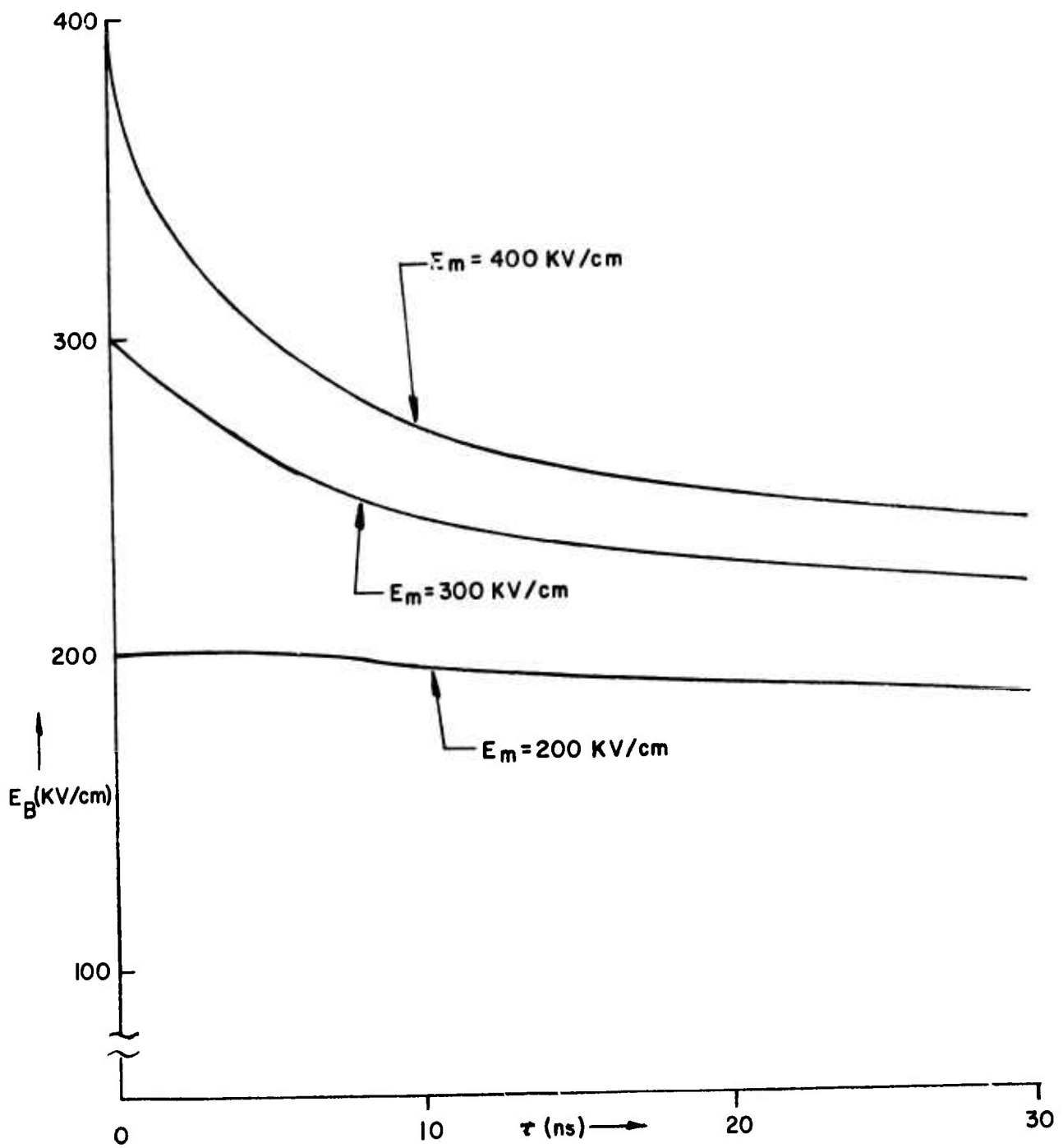


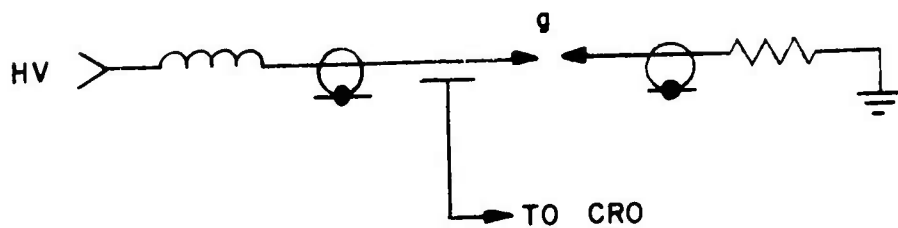
FIGURE 13. BREAKDOWN FIELD STRENGTH vs. APPLIED FIELD RISE TIME

Figure 13, this effect is particularly in evidence when larger values of E_m are employed. As a corollary, the statistical time t_s also increases with larger values of the applied field rise time.

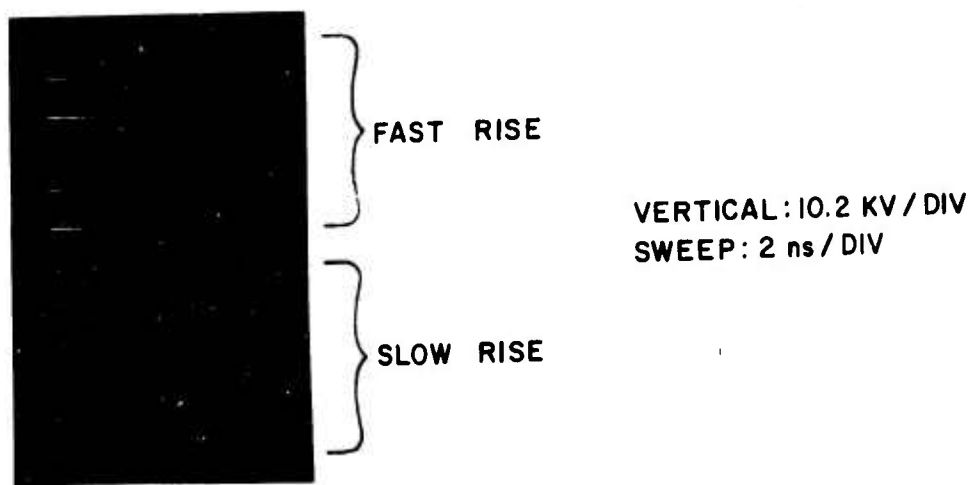
The requirements of relatively slow charging in the frozen wave generator, together with the above analysis, suggest that a practical limit exists for the maximum field strength which can be achieved in the overvolted gaps of the generator. For example, it may be seen with reference to Figure 13 that doubling the source voltage (and thus E_m) produces less than a 50% increase in the breakdown field for applied field rise time greater than 5 ns. Although the analytical model chosen here was for the case of resistive charging, similar results would be expected for resonant charging. In the latter case, $(E_B/E_m)^2$ would be a measure of the charging efficiency. In Figure 13 this ratio is near 1.0 for $E_m = 200$ KV/cm but drops to approximately 0.5 for $E_m = 400$ KV/cm. This suggests that the practical generator should operate at values of E_m toward the lower end of this range. To achieve high operating potential, one is led toward increased gap space. However, because of the gap inductance, the gap space is limited to small values. These factors then pose an upper limit on peak rf power which can be generated. An attempt to quantify this limit is presented in a later paragraph.

Confirmation of the predicted trend toward reduction of the breakdown field strength with increased rise time of the applied field was carried out experimentally using the set-up illustrated in Figure 14(a). In this arrangement, a spark gap with fixed spacing ($g = .025$ in) was overvolted through an inductor as indicated. The rate of rise of the applied field at g was varied by using different values of the charging inductor. The waveform of the applied voltage and the breakdown of g were observed by means of a capacity coupled probe as shown.

Typical test results are shown in Figure 14(b). For the fast rising pulses, the total lag is approximately 5 ns with the breakdown field strength near 200 KV/cm. For the slower rising input pulses, the lag is about 10 ns and the breakdown field is approximately 150 KV/cm. While these breakdown field values are somewhat below those predicted above, the trend toward reduced breakdown



(a) EXPERIMENTAL ARRANGEMENT



(b) TYPICAL TEST DATA

FIGURE 14. RISE TIME DEPENDENT BREAKDOWN STUDY

field strength for slower rising pulses is in accord with the theoretical formulation.

3. POWER LIMITING FACTORS

In attempting to quantify the power limits for the microwave frozen wave generator, an analysis has been performed which parallels that applied to the Travatron generator in a recent investigation.⁽⁷⁾ The analysis considers the limitations due to the switch which are brought about by maximum permissible spark gap overvoltages and by switch inductance. The switch function is assumed to be one in which the statistical lag time allows the spark gap to be overvolted for the period of time required for establishing the frozen wave profile. For reasons cited above, this time must be several times the rf period of interest. For a 1 GHz generator, the charging time is then on the order of 10 ns or more. From the previous analysis and experimental tests, the applied field is required to be near or somewhat below 200 KV/cm, typically, for reliable and efficient operation. Thus, the peak voltage $2 V_0$ appearing across the gap d must be less than $2 \times 10^5 d$ volts, where d is expressed in centimeters. Thus, the inequality:

$$V_0 < 10^5 d \quad (18)$$

The formative time component of the switching lag is extremely small⁽⁴⁾ in overvolted gaps with applied fields on the order of 10^5 volts/cm, and may be neglected as it was in the analysis of the Travatron. However, the rise time of the switch as limited by inductance may be appreciable, thus imposing a limit on the gap space d . To estimate this limit, the transmission line switch rise time t_r is required to be less than one quarter rf period. With the simplifying assumption that the complex impedance of the switch can be represented by the inductance of the spark channel, the inequality becomes

$$t_r = 2 L/Z < 1/4 f_0 \quad (19)$$

where Z is the transmission line impedance and f_0 is the rf frequency. Using the same approximation as was used in reference (7), the inductance of the spark channel may be written as

$$L \doteq 10 d \text{ (nh)} \quad (20)$$

where d is in centimeters. Substitution in (19) yields

$$d < .0125 Z/f_0 \text{ (cm)} \quad (21)$$

where f_0 is expressed in GHz. The peak power expression (equation (9)) combined with (18) is then simply

$$P < .31 Z/f_0^2 \text{ (MW)} \quad (22)$$

for frequencies near 1 GHz.

The result predicts that the 1 GHz frozen wave generator, while theoretically more efficient than the Travatron, is capable of about one third the peak power which can be derived from the Travatron. The underlying reason rests in the limitation on overvoltage fields sustained by the spark gaps at breakdown for the two devices. In the Travatron, the statistical lag is chosen to be equal to one-half period of rf as opposed to the much longer charging period in the frozen wave generator. The result is that the coefficient in the inequality (18) is correspondingly greater for the Travatron.

Recent investigations suggest, moreover, that the inductance estimate (20) used in the analyses for both generators is seriously in error, perhaps by as much as an order of magnitude with the result that the predicted peak power capability for both Hertzian devices is overestimated. Inspired in part by this realization, a Travatron design approach has successfully evolved recently which employs high pressure such that the roles of statistical and formative lag components in the spark switches are reversed. Thus, very close spaced gaps may be used to maintain small inductance while pressure is controlled to govern closure time. The net result defeats the limits considered in the above analysis. Unfortunately, this approach cannot be applied to the frozen wave generator, since a large statistical lag is required in establishing the basis for UV synchronization.

A comparison of the characteristic switching times for the frozen wave generator and two forms of the Travatron is presented in Table 3. The rise

TABLE 3
 CHARACTERISTIC TIMING REQUIREMENTS FOR THREE HERTZIAN GENERATORS

	Statistical Lag	Formative Lag	Rise Time
Frozen Wave Generator	$t_s \gg T$	$t_f \ll T$	$t_r < T/4$
Statistical Lag Travatron	$t_s = T/2$	$t_f \ll T$	$t_r < T/4$
Formative Lag Travatron	$t_s \ll T$	$t_f = T/2$	$t_r < T/4$

time in each case refers to that portion of the closure time contributed by reactive impedance components in the switches. Experience suggests that the timing requirements applicable to the formative lag Travatron are the most readily achieved. In fact, this latter Hertzian device has exhibited the greatest peak power capability to date.

The experimental work reported in the next section reveals difficulties in attaining a high power, GHz frozen wave generator which have their roots in causes not completely covered by the above analysis. While successful function has been achieved, the peak power and operating frequencies have been below expectation.

SECTION IV EXPERIMENTAL GENERATORS

Several experimental embodiments of the frozen wave generator were investigated in this program spanning a frequency range from 250 MHz to 1.3 GHz. The initial efforts were placed on the higher frequency versions employing the disc and folded line-disc geometries described in Section II.

1. PRELIMINARY GENERATOR

A preliminary model of the microwave frozen wave generator was constructed along the general design pattern illustrated in Figure 6 above. The principal objective in this case was to test the concept and function of the curved strip line design with centrally located UV triggering. A four-gap device was constructed for this purpose according to the schematic of Figure 15. In this simple breadboard, two curved stripline segments are resonantly charged by the discharge of a transfer capacitance C_t through the main gap g_o and the two equal inductors L_1 and L_2 . A third segment is held at ground potential by means of inductor L_3 . The capacitance C_m is charged simultaneously with the two frozen wave segments, but the UV emitting master gap g_m is adjusted for a self-breakdown voltage below that of gaps g_1 through g_4 . In the physical layout (Figure 16) g_m is located centrally so that the emitted UV propagates along equal air paths to the frozen wave switches. A transmission line short is located immediately behind g_4 to totally reflect the backward propagating (regressive) wave.

In the experimental device the one-way transit time in each segment was designed to be 0.4 ns. The theoretical waveform is then as illustrated in Figure 16 (b). It consists of two positive pulses for the progressive wave and two inverted, reflected pulses for the regressive wave. The typical experimental waveform is also indicated in the figure. Generally, the positive pulses in the waveform were observed with reasonable stability when many pulses were superimposed. From this observation it could be concluded that switches g_1 through g_4 were indeed synchronized by the UV master gap. As further evidence, the waveform lost all of its stable structure when the UV radiation from g_m was

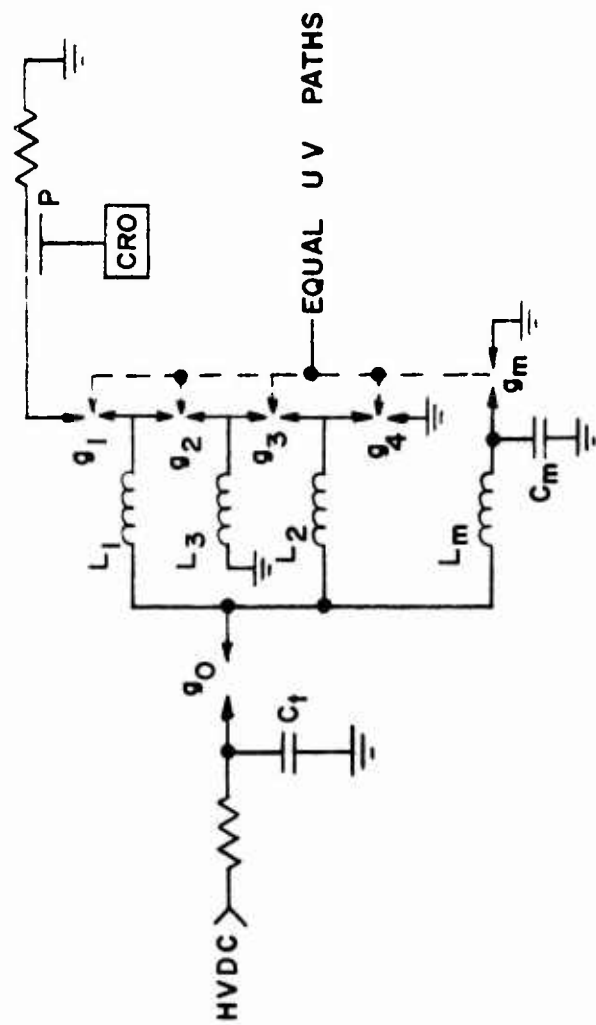
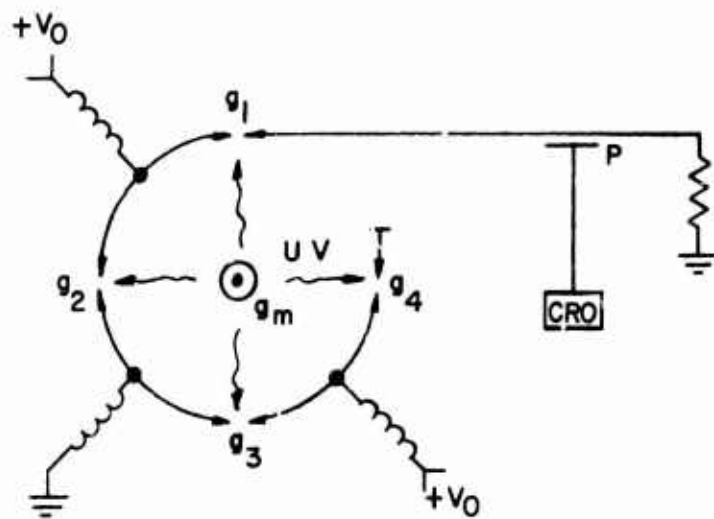
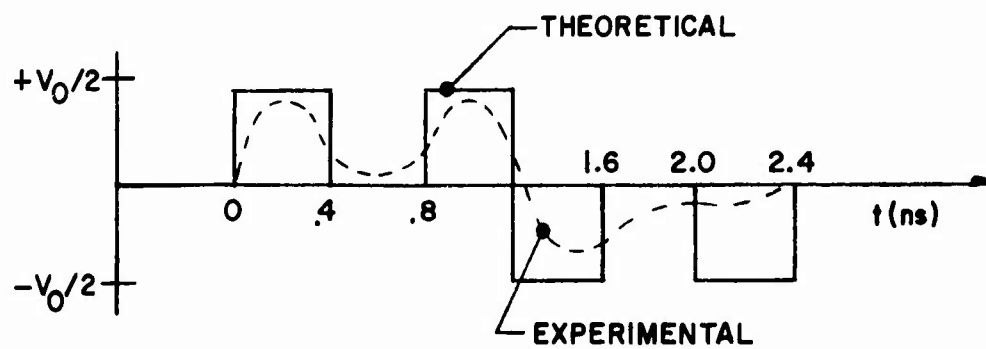


FIGURE 15. PRELIMINARY GENERATOR ELECTRICAL SCHEMATIC



(a) EXPERIMENTAL ARRANGEMENT



(b) OUTPUT WAVEFORM

FIGURE 16. PRELIMINARY CURVED LINE GENERATOR

blocked. The actual synchronization jitter was estimated to be approximately 100 ps.

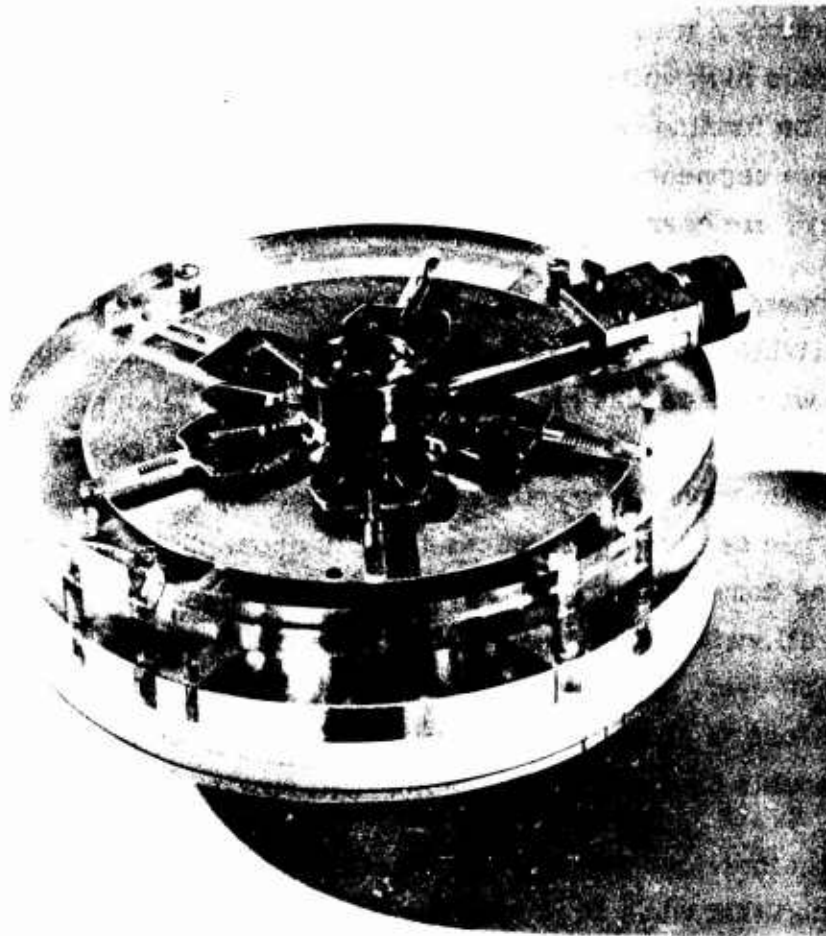
In spite of the fact that g_1 through g_4 were apparently functioning nominally, the regressive wave was of very poor quality. Since its low amplitude and lack of rf structure could not be attributed to switch jitter for the reason cited above, the degradation was thought to be due to ineffectiveness of the rf short or to the inability of the spark switches, when closed, to provide a low loss, distortionless propagation path for the regressive wave.

2. TEN CYCLE, 1.3 GHZ MODEL

Based upon the qualified success of the preliminary generator, a ten cycle, 1.3 GHz generator was constructed following the folded line design approach presented in Section II. The physical design of the generator is illustrated in Figure 7, above. Figure 17 is a photograph of the device with the upper ground plane and dielectric removed.

This generator employs Lucite dielectric in which are embedded five folded line segments on either side of a common, central ground plane. The total length of each segment is 6 cm, corresponding to one half-wavelength at 1.3 GHz. The upper, positively charged segments are switched to the lower, negatively charged segments by means of adjustable spark gaps running vertically through the structure. The current path therefore alternates between the upper and lower groups of segments. The final spark gap in the upper group connects the structure to the output line as shown in Figure 17. A similar gap in the lower group switches the line to ground to reflect the regressive wave. Each segment is charged through the small inductors visible in the photograph.

Following the scheme indicated in Figure 7, a master spark gap is located at the center of the circular array of slave gaps. The latter gaps all lie on a radius of 1.0 in. from the master gap, which is well within the limits prescribed by the previously reported jitter experiments. The master gap is independently adjustable to fine tune its timing relative to the pulse charge applied to the line segments.



SCALE: 1:2 APPROX

FIGURE 17. TEN CYCLE, FOLDED LINE
GENERATOR

To ensure simultaneity in bipolar charging of the frozen wave profile in this generator, a transmission line transformer was employed to generate two simultaneous high voltage pulses of opposite polarity from the discharge of a single pulse forming line. When applied through the charging inductors the frozen wave segments, as well as the small capacitance associated with the master gap, are charged on a time scale of 2 - 3 ns.

In operation, this frozen wave generator model was not completely successful. While strong optical coupling between the master gap and the array of frozen wave gaps was clearly established, no switch adjustment was found for which the generator would produce a complete waveform. Instead, the characteristic waveform consisted of only three to four damped cycles of the rf signal. In search of the causes for this apparent attenuation of the rf signal, a time domain reflectometer measurement was performed on the rf structure with all switches closed. The impedance variations were less than ± 50 ohms. Moreover, prior experience with the Travatron has not indicated an appreciable loss in similar discontinuities even with propagation through active spark channels having the dimensions (gap space \doteq .020 in) used here.

In the previous section, the statistics of UV triggering were examined. It was noted that when large numbers of switches are required to be synchronized, the shapes (higher moments) of the lag time distribution curves are critical to performance of the frozen wave generator. Thus, the relatively rare occurrences of a self-firing gap or that of a large lag time are not so rare when the many switches of the generator are considered. The result of either event is that the first half cycle of rf will appear near its full amplitude while all others will arrive with progressively diminished amplitude. Higher overvoltage levels favor premature self-breakdown, while lesser levels favor longer lag times. In the generator model, no condition could be found which, in effect, would narrow the optical triggering lag time spread. A related and complicating effect was also thought to be due to the resonant charging scheme. Small differences in path lengths or inductance values in the distribution network can lead to irregular charging waveforms which, in turn, can provide irregular overvoltage and optical trigger performance. As evidence of this factor, later

experiments with lower frequency generators showed marked performance improvement when resistive charging was employed.

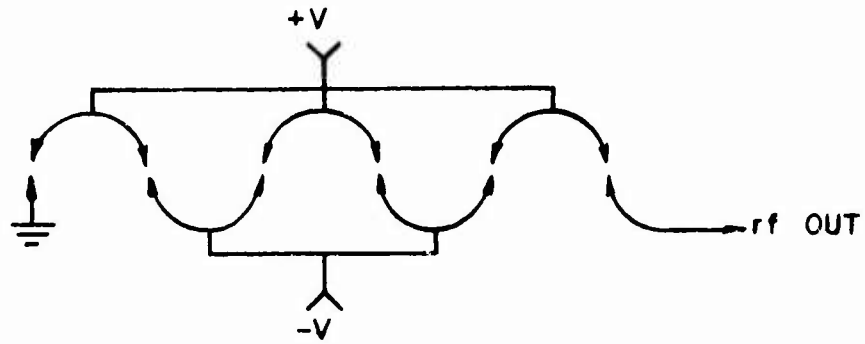
The difficulties with this generator led to the series of experiments described in the next paragraphs. These investigations turned to lower frequency versions of the frozen wave generator where design flexibility can be achieved using coaxial cable.

3. COAXIAL GENERATORS

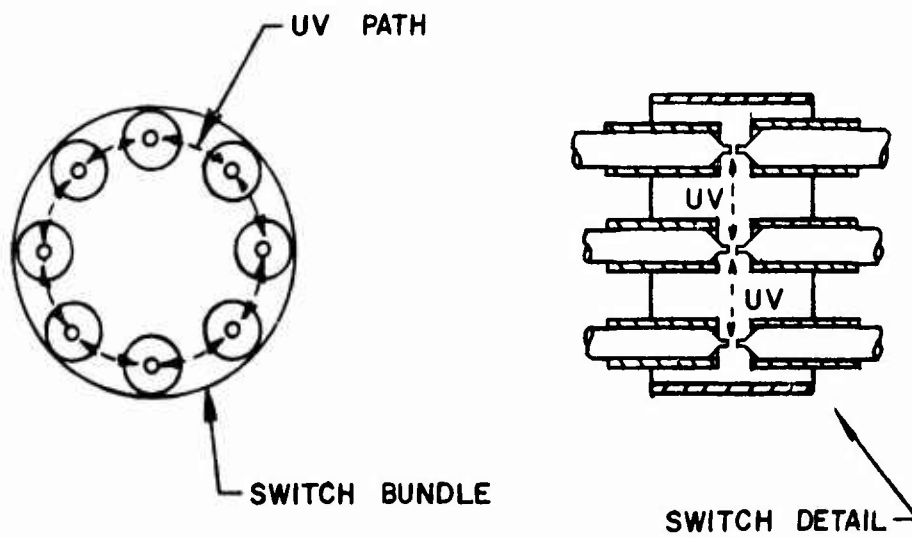
Several experimental frozen wave generators employing coaxial cables were constructed in the program to test the basic design approach at lower frequencies, where problems of trigger jitter, uniformity of line impedance, rf isolation of the charging circuit and switch inductance are all eased. The basic experimental approach was to construct generators having only small numbers of line segments and switches and to expand the number step-wise toward the more complete generator. The initial design frequency was 250 MHz, while later experiments attempted to extend performance to 500 MHz and higher.

The generic experimental arrangement for the laboratory work is illustrated in Figure 18. The electrical schematic is identical to that for the generators described previously. However, the switch arrangement for the cable generators involves a closely spaced bundling of the coaxial switches so that, in general, the spark switches are coplanar and lie in a circle of small diameter. For most of the experimental work, the timing of the switches was accomplished by mutual UV triggering circumferentially as indicated. The coaxial cable used was RG-8 with 16 in segment lengths for 250 MHz generators. The input charging pulse was injected at the midpoint of each section through a break in the outer conductor. Resistive charging was employed in most cases.

Figure 19 illustrates the simplest configuration investigated to generate a single cycle at 250 MHz. The arrangement involves only one charged segment and two synchronized gaps. The segment in this case was charged in 40 ns to a peak voltage of 6 KV with g_1 and g_2 adjusted to approximately .06

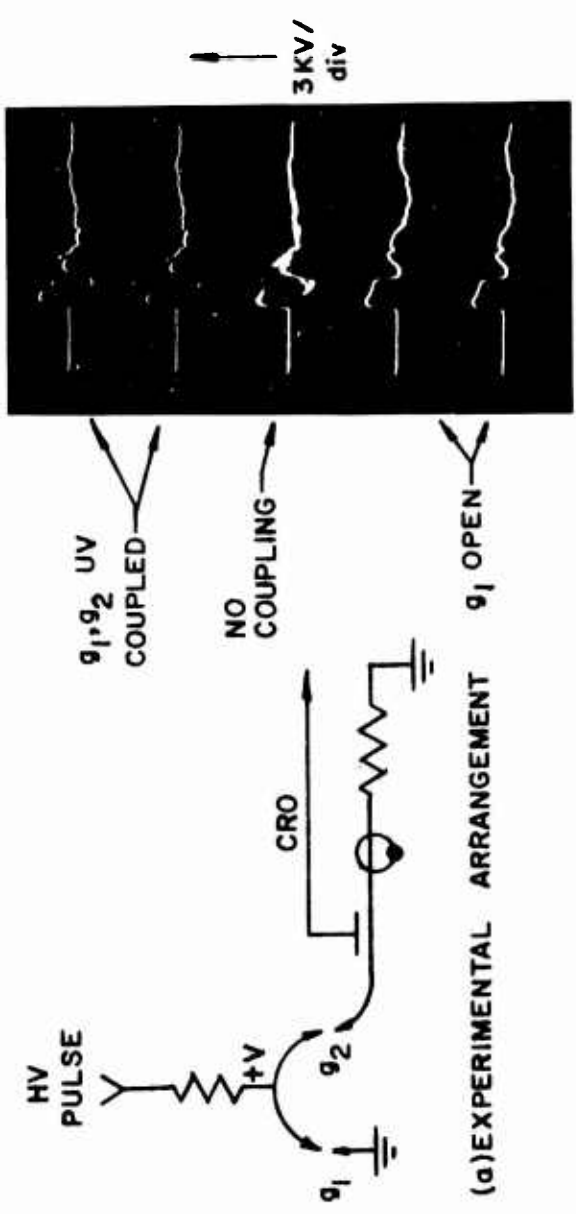


(a) ELECTRICAL SCHEMATIC

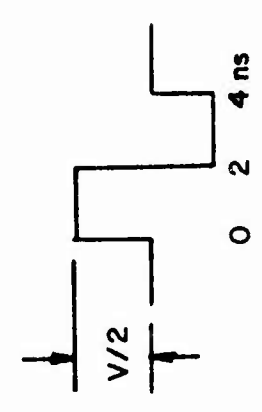


(b) SWITCH ARRANGEMENT

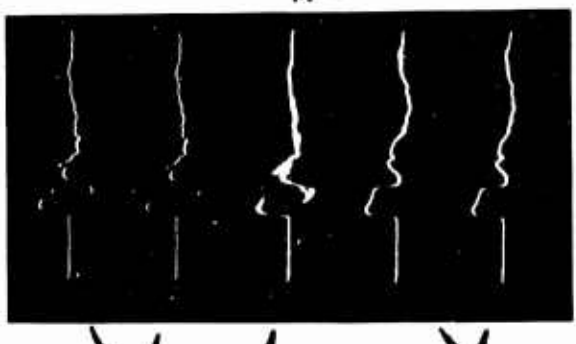
FIGURE 18. COAXIAL FROZEN WAVE GENERATOR



(a) EXPERIMENTAL ARRANGEMENT



(b) IDEAL WAVEFORM



(c) OBSERVED WAVEFORMS

FIGURE 19. SINGLE CYCLE GENERATOR

cm. The peak applied field strength was then near 100 KV/cm. The separation of g_1 from g_2 was less than 1.0 in to obtain appropriate UV coupling and a path delay (~ 1 ns) which was small compared to the rf period.

The ideal waveform for this arrangement is illustrated in Figure 19(b). Thus, when g_1 and g_2 close simultaneously, a positive progressive wave of 2 ns duration is followed immediately by the inverted negative image via the reflected regressive wave.

The actual output from the one cycle generator is shown in Figure 19(c) for three operating conditions. In each case approximately 30 sweeps are superimposed to indicate stability. The first two traces obtained with UV coupling of g_1 and g_2 exhibit a high degree of stability in the synchronization of the spark switches and a close resemblance to the idealized waveform. The role of UV coupling in achieving this stability is illustrated in the third trace. In this case, the optical path is blocked with the result that an unstable waveform is seen with individual sweeps indicating a wide span in the relative timing between g_1 and g_2 . (Note that the initial portion of the waveform is stable in all cases. This is due to the fact that the sweep is triggered from the input signal within the CRO.) The last two traces shown are for the case where g_1 is opened to the point where it is not triggerable. In this case, the charged segment becomes a simple, end switched, charged line and should, therefore, produce a square pulse whose width equals the two-way transit time in the segment (4 ns). The output is seen to resemble this waveform.

The overall results of this experiment are in excellent accord with theory and the previous empirical findings regarding UV synchronization. The trigger stability is very good with an estimated trigger delay and jitter less than 75 ps. This characteristic is of considerable importance as it suggests the practicality of eliminating the master timing gap for the lower frequency generator of this type. The actual condition which must be met is that the delay and jitter must be less than the transit time in the segment or one-half period.

Another important observation in this experiment is the equality in amp-

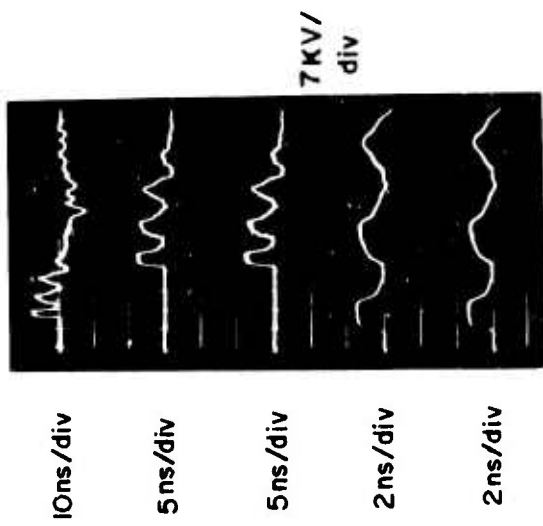
litude in the positive and negative portions of the pulse. This demonstrates that the switches have passed both progressive and regressive waves without degradation.

A three cycle, unipolar generator was constructed according to the schematic of Figure 20(a). In this case, three segments were charged positively, while two segments were simply held at ground potential. For viewing purposes, the rf short for mirroring the regressive wave was placed at the end of a 5 ft cable to provide 15 ns separation of the progressive and regressive waves. The idealized waveform for this generator is then as shown in Figure 20(b).

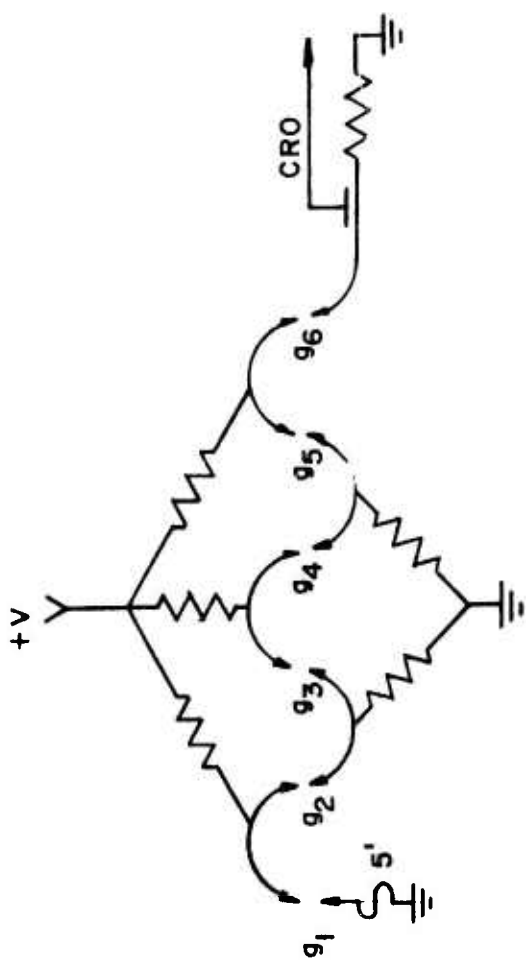
The observed waveforms (30 sweeps/trace) illustrate a high degree of stability and repeatability, thereby demonstrating the ability to lock reliably the closure of multiple spark switches (six in this case) to very high tolerance. The time extent of the three positive pulses is seen to be approximately 11.5 ns as compared to the theoretical value of 10 ns. This apparent stretching of the pulse can be accounted for by the cumulative path and trigger delay of the circumferentially propagating UV signal. This effect also tends to degrade the signal shape somewhat according to observation. The delayed regressive wave is seen to have suffered both loss and distortion which can only be accounted for by propagation through the switch structures. Note that the last cycle of the regressive wave passes each switch twice with reversing polarity.

Figure 21 illustrates similar results for a generator possessing eight spark switches. The gradual degradation of the waveform and loss associated with the regressive wave are again in evidence. Moreover, in this case it was not possible to achieve the extremely low jitter evidenced in the six gap generator.

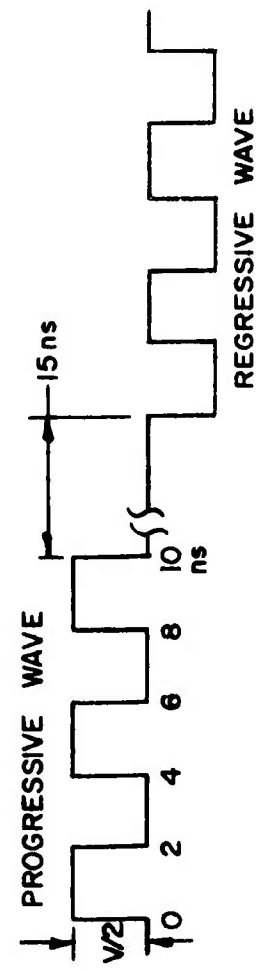
The preceding set of experiments established the feasibility of simultaneously triggering up to eight spark switches in the frozen wave generator. In order to achieve high generator efficiency, it is necessary to charge adjacent segments of the device to opposite polarity. Accordingly, the follow-



(c) OBSERVED WAVEFORM

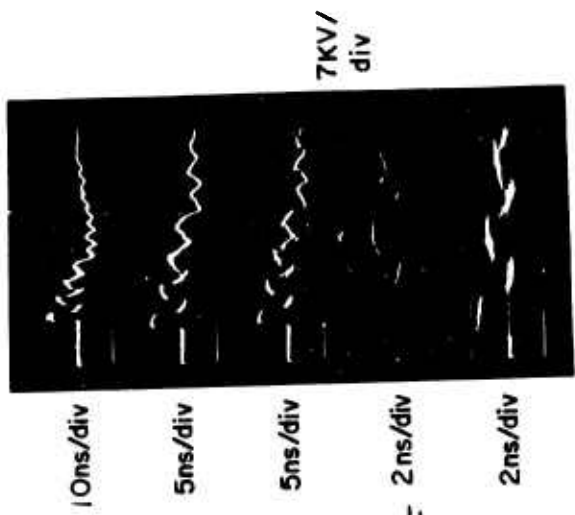


(a) EXPERIMENTAL ARRANGEMENT

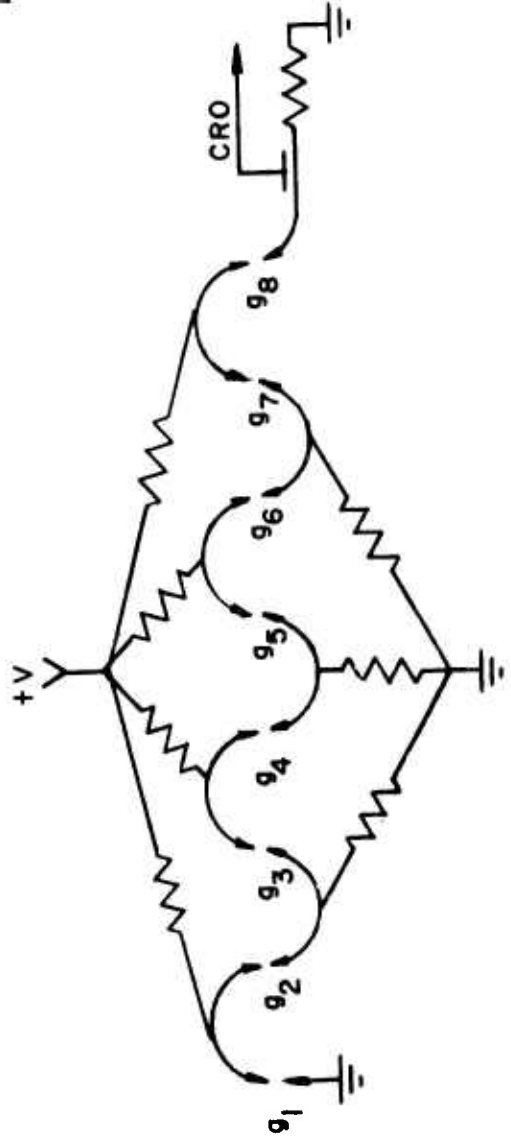


(b) IDEAL WAVEFORM

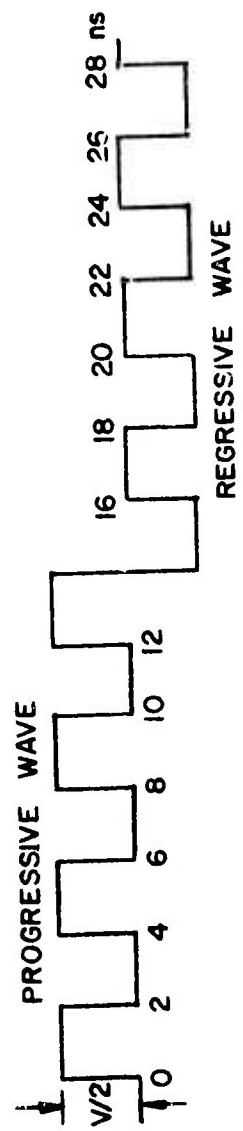
FIGURE 20. THREE CYCLE UNIPOLAR GENERATOR



(c) OBSERVED WAVEFORM



(a) EXPERIMENTAL ARRANGEMENT



(b) IDEAL WAVEFORM

FIGURE 21. FOUR CYCLE UNIPOLAR GENERATOR

ing set of experiments was undertaken to investigate the more complex, bipolar operation.

The simplest experiment is illustrated in Figure 22. Here, a two segment generator was constructed with three spark switches. Bipolar pulse charging was accomplished by means of the cable transformer method to assure simultaneous application of the charging pulses. The rf short in this case was delayed through a 1.5 ft cable as indicated.

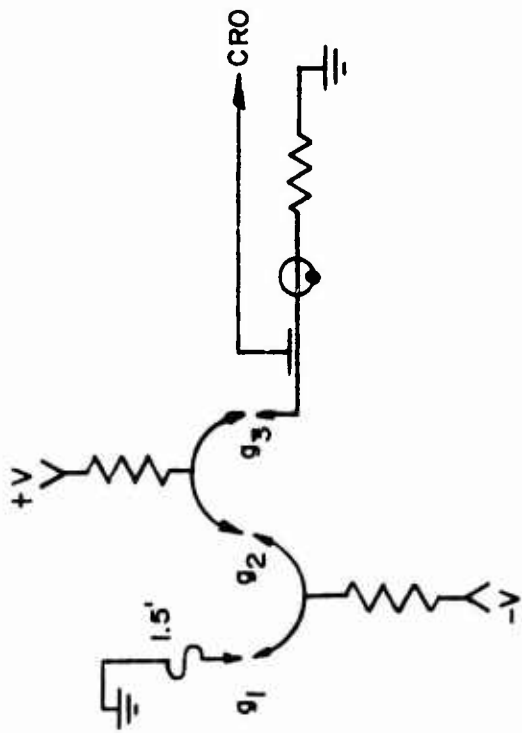
The bipolar generator introduces a complexity with regard to switch design which did not exist in the unipolar devices. This may be seen with reference to 22(a). When the frozen wave is established, the magnitude of the voltage drop across g_1 and g_3 is V , while across g_2 it is $2V$. Thus, the switches in this and all bipolar cases are not identical.

The experimental results for this generator, as seen in the five CRO traces (each contains multiple sweeps), are close to the ideal waveform. The basic ability to accomplish bipolar charging and synchronous switching is thus demonstrated.

The next more complex bipolar generator is depicted in Figure 23. In this case, four segments and four spark switches are employed with an open circuit to reflect the regressive wave without phase change. A four cycle waveform is then produced as indicated in Figure 23(b).

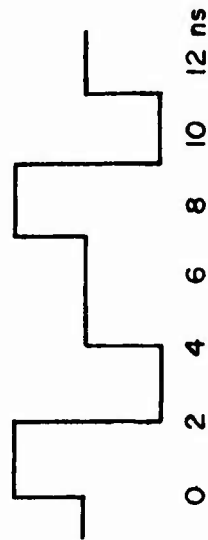
The observed waveform departs only slightly from the ideal. The first two cycles are correct in timing and amplitude. The fourth cycle, which is part of the regressive wave, is somewhat reduced in amplitude. However, the open circuit apparently reflects the pulse quite well.

In the next model, shown in Figure 24, a five segment, six gap generator was constructed. In this case, the pulsed bipolar charging was through small inductors as indicated, having the primary effect of decreasing the charge time to approximately 10 ns. The results show excellent stability. In total, the observed waveforms include 150 individual sweeps with no evidence of even a single misfiring switch. Apparently, a five cycle generator at this frequency is

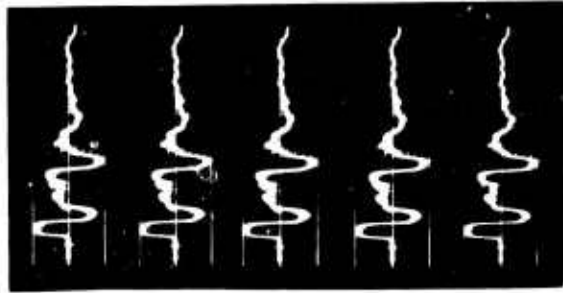


(a) EXPERIMENTAL ARRANGEMENT

PROGRESSIVE
WAVE



(b) IDEAL WAVEFORM

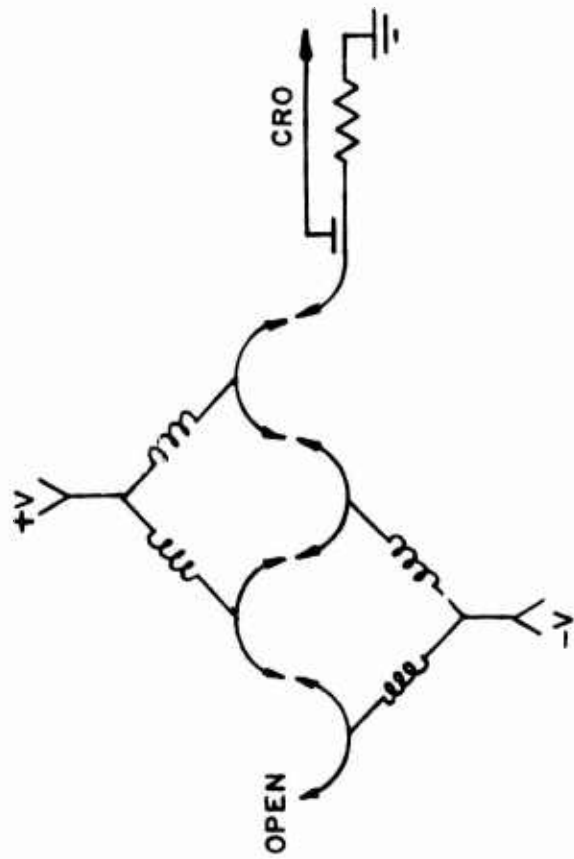


2KV/div

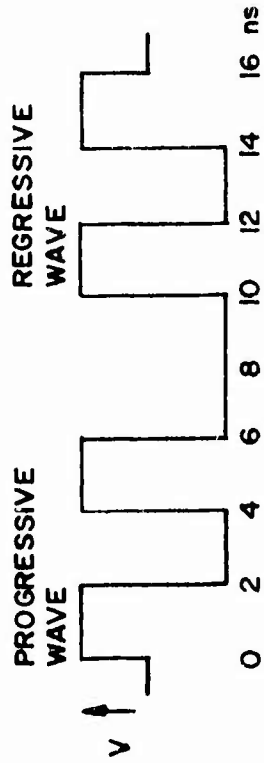
5 ns/div

(c) ACTUAL WAVEFORM

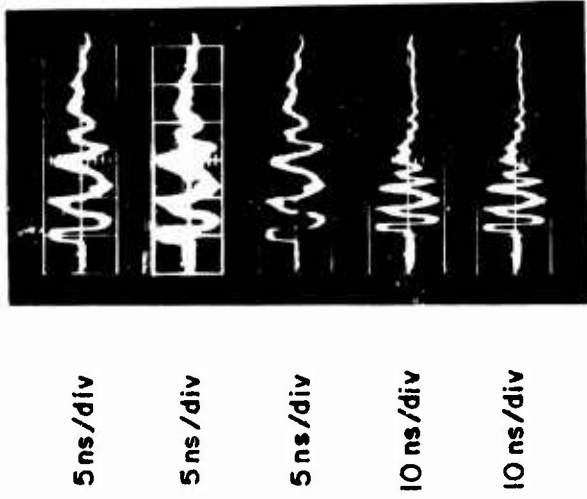
FIGURE 22. TWO CYCLE BIPOLAR GENERATOR



(a) EXPERIMENTAL ARRANGEMENT

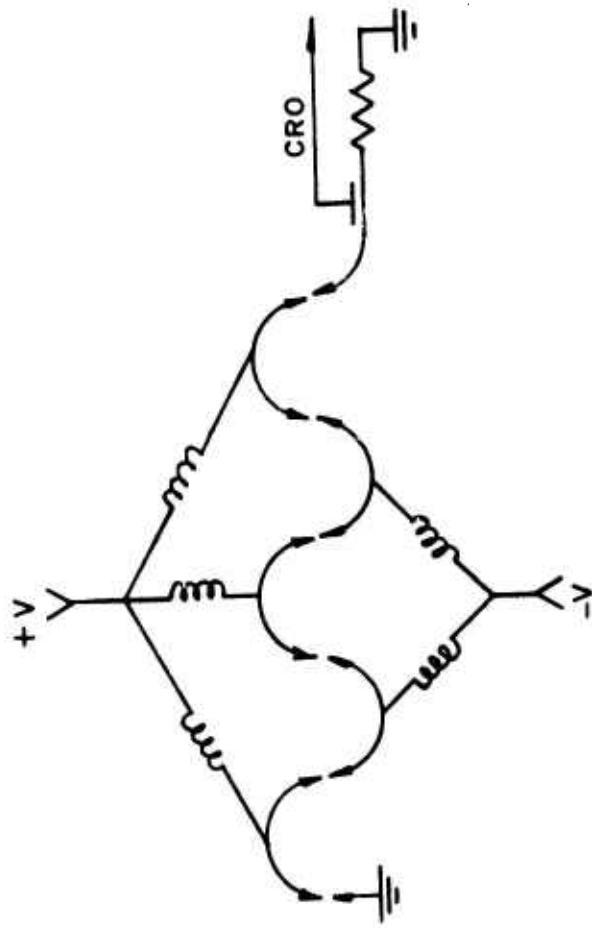


(b) IDEAL WAVEFORM

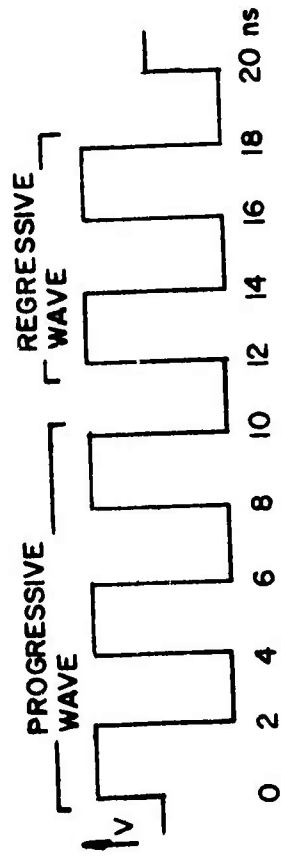


(c) ACTUAL WAVEFORM

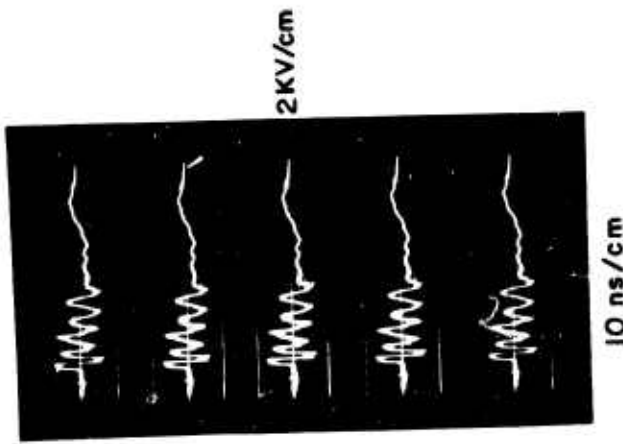
FIGURE 23. FOUR CYCLE BIPOLAR GENERATOR



(a) EXPERIMENTAL ARRANGEMENT



(b) IDEAL WAVEFORM



(c) ACTUAL WAVEFORM

FIGURE 24. FIVE CYCLE BIPOLAR GENERATOR

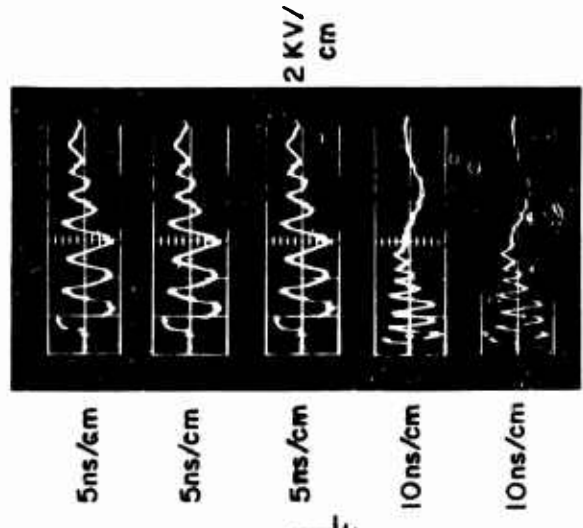
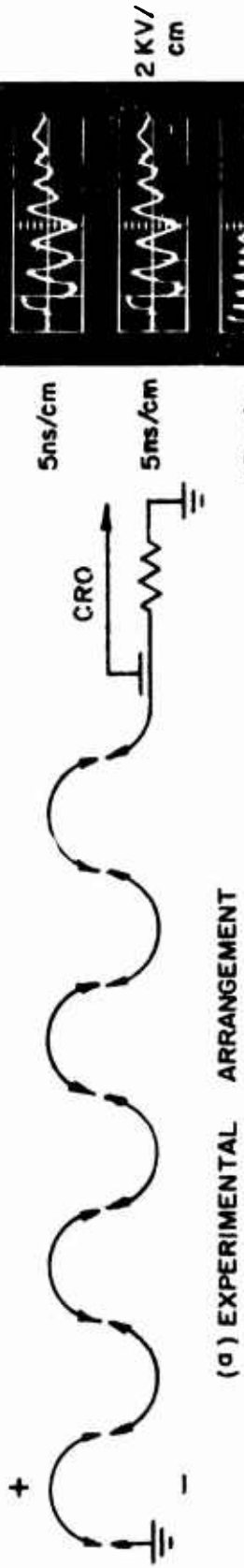
is quite feasible.

An eight cycle generator was constructed as shown in Figure 25. The progressive wave in this case is produced with uniform amplitude and correct timing. However, the regressive wave is seen to decay to less than half amplitude and the eighth cycle is virtually absent. The apparent attenuation may be owing to propagation loss in the switches. The loss mechanism is thought to be caused by the relatively low modulator voltage and consequently low travelling wave energy in the spark switches. One result of this would be the production of weakly ionized plasma in each switch and consequent lossy spark discharges. Attempts to employ a modulator technique with higher power capabilities such as that illustrated in Figure 8 were met with considerable difficulty in achieving the necessary simultaneity in dual polarity charging. While this is overcome in the cable transformer modulator, the method divides operating voltages to the point where high power levels are not readily tenable.

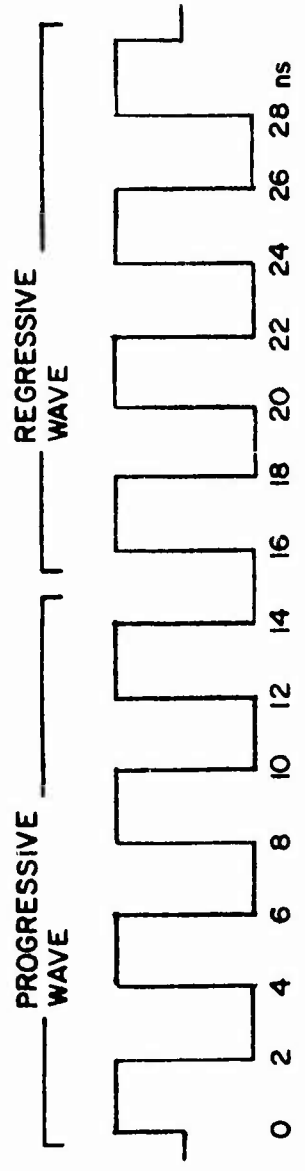
The investigation of coaxial frozen wave generators was extended to higher frequency by constructing the eight cycle, 500 MHz generator shown in Figure 26. At this higher frequency, it was anticipated that the problems associated with spark gap delay, jitter, switch inductance, and impedance discontinuities would all be more serious.

Figure 26 shows the experimental configuration, the ideal waveform, and the observed waveforms for the 500 MHz generator. Performance of the device shows that a progressive wave is produced, albeit with discernible switch jitter. However, the regressive wave does not appear at all at the output. Again, the attenuation of the regressive wave is apparently switch loss which is evidently greatest for g_1 .

While the 500 MHz generator shows promise, the degradation of the regressive wave is pronounced as compared to results at 250 MHz. Moreover, with this trend, it is not difficult to understand the poor performance noted earlier with the 1.3 GHz generator. Following the same trend, it would be reasonable to expect considerable improvement in performance at lower frequencies, say 100 MHz.



(c) ACTUAL WAVEFORM

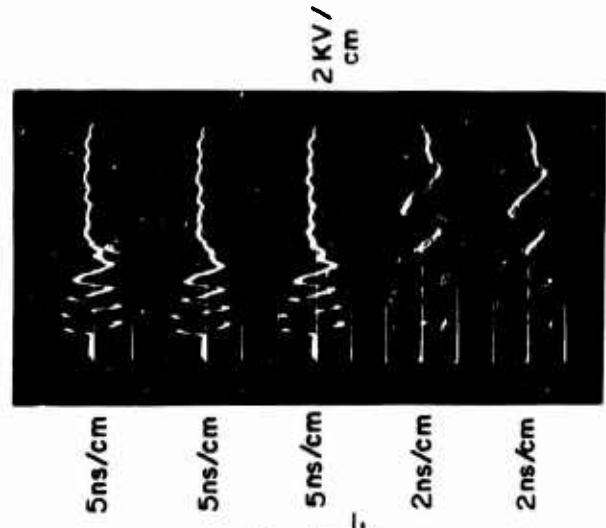


(b) IDEAL WAVEFORM

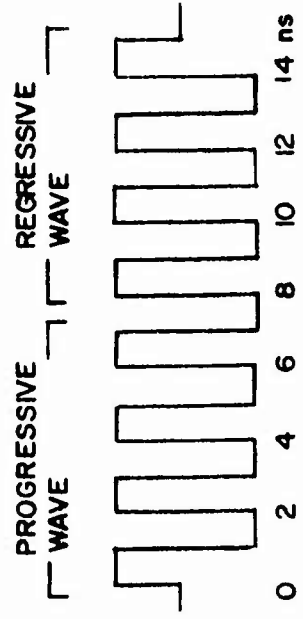
FIGURE 25. EIGHT CYCLE BIPOLAR GENERATOR



(a) EXPERIMENTAL ARRANGEMENT



(c) ACTUAL WAVEFORM



(b) IDEAL WAVEFORM

FIGURE 26. EIGHT CYCLE 500 MHz GENERATOR

SECTION V
SUMMARY AND RECOMMENDATIONS

This investigation has encompassed many of the development problem areas associated with extending the capability of the frozen wave generator to frequencies in the UHF and low microwave range. The program has resulted in successful demonstration of breadboard models of the generator operating at 250 MHz and above. Thus, a two order of magnitude extension in frequency capability has, in fact, been achieved over the prior art. Attempts to attain yet higher frequency performance at 500 MHz and 1.3 GHz were met with lesser success. However, the theoretical and practical implementation difficulties have been identified and assessed.

To meet the unique switching requirements of the frozen wave generator, a spark gap switching technique using ultraviolet light pulses for control was adopted at the outset. The switch method is the only one which could be identified as possessing all of the required properties of voltage handling, fast closure, and subnanosecond jitter. As a part of this investigation, an experimental and analytical study of the UV triggered gap was undertaken. Ultimately, the reliable jitter-free synchronization of numbers of spark switches as configured in the frozen wave generator was demonstrated.

The frozen wave generator and the Travatron are similar Hertzian devices in some respects. It has, therefore, been an aim of this program to establish comparative evaluation where possible. Prior to this investigation, the attractive characteristic of the frozen wave generator was its theoretically higher efficiency. In practice, this feature is largely offset by implementation difficulties. At frequencies near 1GHz, past experience has established the Travatron as a workable, reliable device. At this frequency, the frozen wave generator is confronted with serious difficulty especially with regard to the need to establish the frozen wave profile rapidly. As the frequency is reduced, the implementation problems ease for the frozen wave generator while, for the Travatron, implementation actually becomes more difficult below about 200 MHz. Although a 100 MHz device was not modeled in this program, it is believed that a high efficiency, relatively simple, frozen wave generator can be

built at this frequency or below.

The further development of the frozen wave generator is inevitably tied to the fundamental switching mechanism chosen. Further work should therefore be applied to the switching means. In the spark switch, the most deficient area at present has to do with accurate trigger and synchronization means. Considerable understanding now exists regarding UV triggering of overvolted gaps, but this constitutes only one of several candidate schemes. The number of workable schemes appears to increase as one looks toward lower frequency application. At 100 MHz, for example, triggering alternatives employing third electrodes (field gradient vs trigatron) and lasers are worthy of consideration. Relaxation of the high power requirements would permit broadening to include semiconductor devices.

REFERENCES

1. E. S. Weibel, Rev. Sci. Instr., 35, 173 (1964)
2. A. Lietti, Rev. Sci. Instr., 36, 13 (1965)
3. J. M. Proud and H. J. Huber, RADC-TR-67-400
4. P. Felsenthal and J. M. Proud, Phys. Rev. 139, 1796 (1965)
5. US Patent No. 3,484,619
6. J. M. Proud et al., RADC-TR-68-254
7. J. M. Proud and W. H. McNeill, RADC-TR-73-227
8. US Patent No. 3,521,121
9. US Patent No. 3,681,656
10. US Patent No. 3,748,528
11. J. M. Proud et al., AFAL-TR-72-41
12. H. Hertz, An. d. Physik 31, 983 (1887)



MISSION
of
Rome Air Development Center

RADC is the principal AFSC organization charged with planning and executing the USAF exploratory and advanced development programs for electromagnetic intelligence techniques, reliability and compatibility techniques for electronic systems, electromagnetic transmission and reception, ground based surveillance, ground communications, information displays and information processing. This Center provides technical or management assistance in support of studies, analyses, development planning activities, acquisition, test, evaluation, modification, and operation of aerospace systems and related equipment.